Nanoscale Horizons

REVIEW

View Article Online
View Journal | View Issue

Cite this: *Nanoscale Horiz.*, 2018, 3, 74

2D transition metal dichalcogenide nanosheets for photo/thermo-based tumor imaging and therapy

Hang Chen,[a] Tianjiao Liu,[a] Zhiqiang Su,*[a] Li Shang*[b] and Gang Wei*[c]

Two-dimensional (2D) graphene-like nanomaterials show wide applications in the fields of nanodevices, sensors, energy materials, catalysis, drug delivery, bioimaging, and tissue engineering. Recently, many studies have been focused on the synthesis and application of 2D transition metal dichalcogenide (TMD) nanosheets for various biomedical applications. In particular, 2D TMD nanosheets exhibit great advantages for tumor imaging and therapy compared to some traditional nanomaterials due to their high specific surface area, good biocompatibility, easy modification, and ultrahigh light and heat conversion efficiency. In this review, we summarize the recent advances in the synthesis, modification, and photo/thermo-based tumor imaging and therapy of 2D TMD nanosheets. The important studies on tumor bioimaging with TMD nanosheets, such as X-ray computed tomography, magnetic resonance imaging, and photoacoustic imaging, are demonstrated and discussed. In another section, the physical photothermal and photodynamic therapies as well as the pharmacological therapy of tumors with TMD nanosheet-based nanohybrids are introduced. It is expected that this work will be valuable for readers to understand the synthesis and modification of TMD nanosheets to design novel 2D functional nanomaterials for photo/thermo-based tumor imaging and therapy in one aspect, and in another aspect will extend the applications of TMD-based nanomaterials in materials science, analytical science, electrocatalysis, tissue engineering, and others.

Received 4th October 2017,
Accepted 31st October 2017

DOI: 10.1039/c7nh00158d

rsc.li/nanoscale-horizons

1. Introduction

Cancer is one of the serious diseases increasingly threatening human health. Despite widespread use in clinics for a long time already, traditional chemotherapy and radiotherapy possess serious drawbacks including huge damage to the human body and high recurrence rate, and thus they cannot meet the needs of biomedical treatment of cancers. With the development of nanotechnology, it is possible to break through the barriers of cancer treatments by using some functional nanomaterials and corresponding curing techniques.[1] In the past few decades, various nanomaterials with different dimensions, such as zero-dimensional (0D) nanoparticles and nanodots,[2,3] one-dimensional (1D) nanowires[4] and nanotubes,[5] two-dimensional (2D) nanosheets,[6–8] and three-dimensional (3D) scaffolds,[9] have been extensively prepared and used for promising applications in biomedical fields including cell imaging, tumor therapy,[8,10] and drug delivery.

2D graphene and graphene-like materials possess high surface area, good biocompatibility, strong corrosion resistance, and high stability. Previous studies have indicated that 2D graphene-like materials showed potential biomedical applications with exciting performance.[11] Transition metal dichalcogenides (TMDs) are a family of graphene-like materials consisting of over 40 compounds with the generalized formula of MX_2.[12] Representative TMD materials include MoS_2,[13–16] WS_2[17] and $MoSe_2$,[18] which can be prepared by different approaches like mechanical stripping, lithium ion intercalation, liquid stripping, and meteorological precipitation. TMD nanosheets synthesized using different methods are suitable for various research fields such as electrochemistry, catalysis, energy storage, biomedicine, and so on.

TMD nanosheets have also shown great potential for biomedical applications such as drug delivery as well as tumor imaging and therapy due to several distinct advantages. Firstly, TMD nanosheets possess a high specific surface area and a large number of active sites, which are favourable for chemical modification, and therefore biomolecules can be conjugated onto TMD nanosheets to improve their biocompatibility.[19] Secondly, TMD nanosheets can be easily doped with paramagnetic particles for tumor bioimaging, such as computed tomography (CT),[20] magnetic resonance (MR) imaging,[21] and

[a] State Key Laboratory of Chemical Resource Engineering, Beijing University of Chemical Technology, 100029 Beijing, China. E-mail: suzq@mail.buct.edu.cn
[b] State Key Laboratory of Solidification Processing, Center for Nano Energy Materials, School of Materials Science and Engineering, Northwestern Polytechnical University and Shaanxi Joint Laboratory of Graphene (NPU), Xi'an, 710072, China. E-mail: li.shang@nwpu.edu.cn
[c] Faculty of Production Engineering, University of Bremen, D-28359 Bremen, Germany. E-mail: wei@uni-bremen.de

photoacoustic (PA) imaging techniques.[22] Thirdly, TMD materials have ultrahigh light and heat conversion efficiencies, which are perfect for photo/thermal-induced tumor photothermal and photodynamic therapy (PTT/PDT). For example, $MoSe_2$ has revealed a thermal conversion of 57.9%, which is similar to that of gold nanoparticles (AuNPs) for potential applications in PTT/PDT.[23] The adoption of TMD materials could not only solve the problem of surface modification, but also enable a transition from single-modal PDT (or PTT) to dual-modal therapy (PTT + PDT), which shows better therapy performance.[24] Finally, TMD nanosheets show near-infrared (NIR) absorption properties and could act as the photosensitive doping agents in a TMD–polymer hybrid hydrogel system.[25,26] Therefore, controlled drug delivery and release could be achieved by NIR-mediated heating of thermo-sensitive hydrogels.

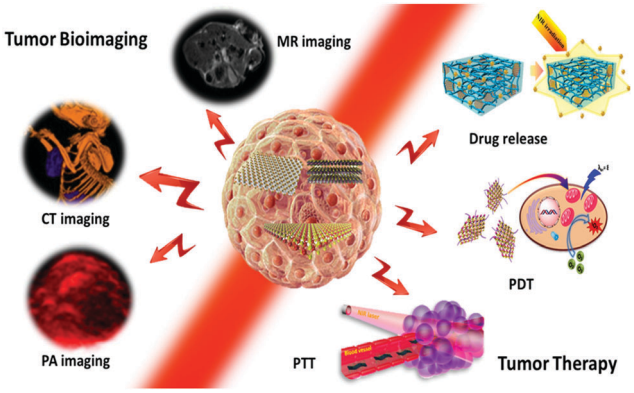

Fig. 1 Schematic illustration of 2D TMD nanosheets for photo/thermo-based tumor bioimaging and therapy.

With the development of chemical synthesis and modification of TMD materials, many studies on the biomedical applications of TMD nanosheets have been reported in the last few years. Previously, several reviews on the synthesis,[27] modification,[28] and biomedical applications of TMD materials have been reported.[12,29–32] For example, Chen *et al.* demonstrated the cancer therapy and bioimaging with 2D TMD nanosheets,[12] and Chimene *et al.* introduced TMDs and transition metal oxides (TMOs) for biomedical applications.[32] Although great achievements have been obtained and a lot of useful knowledge has been acquired from these studies, there is still some space left in order to enrich the content of this emerging topic.

Zhiqiang Su

Zhiqiang Su was born in 1975 and completed his PhD studies in 2005 at the Institute of Chemistry, Chinese Academy of Sciences. After a postdoctoral stay at Tsinghua University, he joined the Beijing University of Chemical Technology in 2007 and was appointed as Full Professor in 2012. In 2011 he studied at Friedrich-Schiller-University Jena, Germany as an experienced research fellow of the Alexander von Humboldt Foundation. His research interests include nanohybrids, biomedical materials, biosensors, and bioelectronics. So far, he has published more than 100 papers in international peer-reviewed journals.

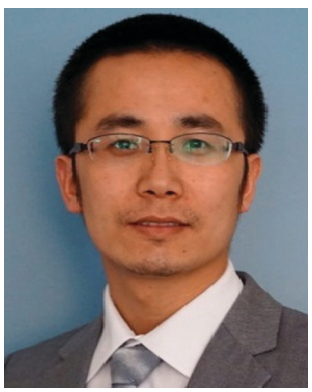

Li Shang

Li Shang received his BS (2004) from Wuhan University and his PhD in Chemistry (2010, supervisor: Prof. Shaojun Dong) from Changchun Institute of Applied Chemistry, Chinese Academy of Sciences. In 2010, he joined the group of Prof. G. Ulrich Nienhaus, Karlsruhe Institute of Technology (KIT), Germany, as a Humboldt fellow and then as a Research Associate. In 2016, he became a Professor in the Center for Nano Energy Materials and School of Materials Science and Engineering, Northwestern Polytechnical University, China. His research interests include fluorescent nanoprobes, biosensors, and nano-bio interactions. Up to now, he has coauthored over 60 peer-reviewed publications in high-impact journals such as Acc. Chem. Res., Mater. Today, Nat. Chem., Angew. Chem., Int. Ed., Adv. Funct. Mater., and Chem. Sci., with total citations over 4000 and H-index: 35.

Gang Wei

Gang Wei received his PhD from Changchun Institute of Applied Chemistry, Chinese Academy of Sciences, China, in 2007. Following his doctoral studies, he worked as the Alexander-von-Humboldt (2007) and Carl-Zeiss (2009) Postdoctoral Fellow at the Friedrich-Schiller-University of Jena, Germany. Since 2012, he has worked as a senior researcher and group leader in the Hybrid Materials Interfaces Group at University of Bremen, Germany. His research interests include two-dimensional nanomaterials, supramolecular self-assembly, sensors and biosensors, as well as single molecule force spectroscopy. Up to now, he has published 100+ papers in the peer-reviewed journals, and the published papers have been cited more than 2400 times with an H-index of 34.

Therefore, in this review, we focus on photo/thermo-based tumor imaging and therapy with 2D TMD nanosheets, as shown in Fig. 1. In Section 2, the synthesis, modification, and various applications of TMD nanosheets are introduced briefly. In Section 3, the recent advances in tumor imaging including magnetic resonance (MR), computed tomography (CT), and photoacoustic (PA) imaging with TMD nanosheets are presented. In Section 4, important cases of tumor therapy (physical PTT/PDT and pharmacological drug therapy) with TMD nanosheets and corresponding TMD-based nanohybrids are demonstrated. It is expected that this work will further guide studies on the design, synthesis, and biomedical applications of novel TMD-based nanomaterials in the future.

2. Synthesis, modification, and applications of TMD nanosheets

In this section, we would like to introduce briefly the main strategies to produce TMD nanosheets, and then summarize the structure and properties of TMD nanosheets prepared using various methods. In addition, the functionalization of TMD nanosheets to combine them with other nanoscale building blocks for extended applications will be demonstrated.

2.1 Synthesis of TMD nanosheets

2.1.1 Mechanical exfoliation. The mechanical exfoliation method is the earliest physical approach to prepare graphene and other 2D nanosheets.[33] Due to weak interactions (such as van der Waals force) between layers, the stacking between layers is not tight enough. Previously, Novoselov *et al.* successfully prepared single-layer graphene, MoS_2, $NbSe_2$, $Bi_2Sr_2CaCuO_x$, and BN, through the mechanical exfoliation of bulk materials.[34] Similarly, 2D TMD nanosheets of single-atomic thickness have also been exfoliated by this method. Recently, Xing *et al.* successfully exfoliated 2D nanosheets, such as MoS_2, BN and graphene, in an atmosphere of NH_3, C_2H_4 and CH_4 gases with high-energy ball milling.[35] 2D nanomaterials become indestructible with high-energy impacts in certain gases due to high absorption of the ammonia and hydrocarbon gases. The mechanochemical reaction of reactive gases resulted in the formation of dangling bonds during milling and chemisorption of reactive species, terminating bonds and preventing the cross-linking of layers upon forming bridging bonds. This milling process in a reactive gas provides a general method to produce different 2D TMD nanosheets with large quantity and high yield.

2.1.2 Ion-intercalation and exfoliation. As a special liquid separation method, ion intercalation-based exfoliation possesses a unique advantage of using ions to react with water and produce a gas to disperse the lamellar gap, thereby weakening the van der Waals forces between the layers, as shown in Fig. 2a.[36] However, there is one potential problem in the subsequent lithiation because it cannot completely replace the liquid peeling. Unlike other 2D materials like graphene, the whole structure of TMD nanosheets is a transition metal atom sandwich between two chalcogenide layers. As a result, TMDs have two different types of

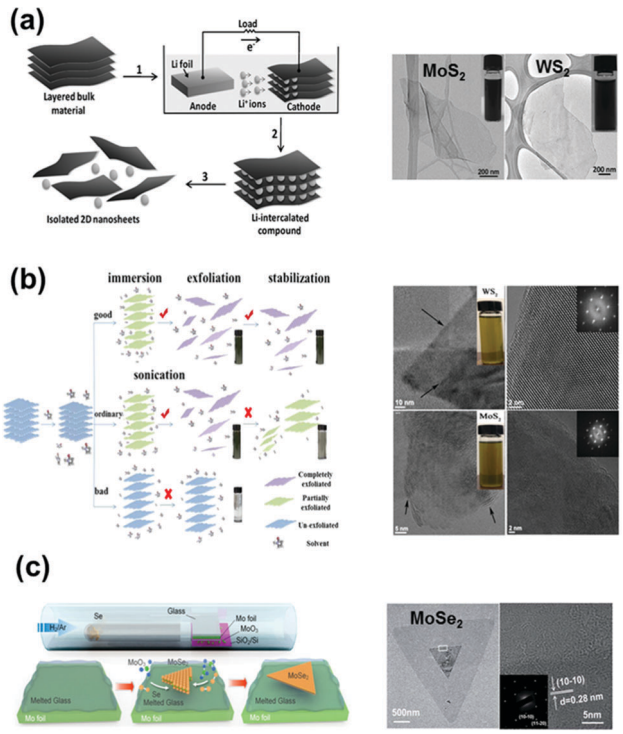

Fig. 2 Typical synthesis methods of TMD nanosheets and corresponding morphologies: (a) electrochemical lithiation preparation of 2D nanosheets from the layered bulk materials. Reprinted with permission from ref. 36. Copyright 2011 Wiley-VCH. (b) Proposed mechanism of an LPE process. An efficient solvent for LPE should have the best matching of surface tension components to the aimed 2D material. TEM images of typical WS_2 and MoS_2 nanosheets. Reprinted with permission from ref. 40. Copyright 2015 American Chemical Society. (c) Scheme showing the CVD process for the synthesis of $MoSe_2$ crystals on molten glass. Reprinted with permission from ref. 43. Copyright 2017 American Chemical Society.

electronic structures, one is a semiconductor hexagonal structure (2H) and the other is a metal phase (1T).[37,38] Generally, the lithium ion intercalation stripping is particularly suitable for the large-scale production of TMD nanosheets, and it is easy to control the key structural/constitutive parameters of 2D TMDs. At present, high quality stripping MoS_2, TaS_2, TiS_2, WS_2, ZrS_2, $NbSe_2$, WSe_2, Sb_2Se_3, Bi_2Te_3, and BN can be obtained facilely. Therefore, this method can be used to produce high-yield TMD nanosheets with good homogeneity, and has proven to be an effective synthesis strategy of 2D TMD nanosheets.

2.1.3 Liquid phase exfoliation. Liquid phase exfoliation (LPE) is another convenient and effective method to prepare TMD nanosheets. The crucial structure and average thickness of the flakes could be easily controlled by adjusting the parameters of the ultrasonic cell disruptor or selecting different surfactants. Previously, Backes *et al.* demonstrated a method to simultaneously determine different parameters of nanosheets such as size, thickness and concentration from an optical extinction spectrum measured from a liquid dispersion of MoS_2 nanosheets.[39] The measurement of concentration is based on the size-independence of the low-wavelength extinction coefficient, while the size and thickness measurements rely on the effect of

edges and quantum confinement on the optical spectra. This detection method enhances the usability of LPE for producing TMD nanosheets. The preparation of 2D TMD nanosheets requires the selection of surfactants that match their surface energies. Shen *et al.*[40] found that the exfoliation efficiency could be enhanced when the ratios of the surface tension components of the applied solvent were close to that of the desired 2D materials. They found that isopropanol as a water-soluble surfactant can effectively meet the tension ratio of TMDs by changing the proportion of isopropanol and water. As shown in Fig. 2b, graphene (thickness 0.4 nm), WS_2 (thickness 1.6 nm), MoS_2 (thickness 1.2 nm), and h-BN nanosheets (thickness 1.3 nm) were successfully stripped by using a mixture of isopropanol and water as the intercalation agent. In addition, Sreshtt *et al.*[41] modelled the solvent phosphorene interactions using an atomistic force field based on *ab initio* calculations and lattice dynamics. Their results accurately reproduced the experimental mechanical properties and solvents whose molecules are planar, particularly near 2D nanosheet surfaces (such as nitrogen methylpyrrolidone (NMP) and DMSO), which behave as molecular wedges to intercalate more efficiently. Furthermore, this intercalation was successful only if the new 2D nanosheet surfaces created by the solvent wedge were stabilized by the sorption forces between the solvent molecules and materials.

2.1.4 Chemical vapor deposition (CVD). CVD is one of the widely-used bottom-up methods for preparing high-quality 2D nanofilms and other layered materials upon deposition on a heated solid or molten substrate *via* chemical reaction between gas-phase small molecules.[42] CVD is particularly suitable for the manufacture of large-sized, thickness controllable, and highly demanded 2D nanosheets. Due to the need of an expensive chemically inert metal as a substrate, the practicability of CVD has been restricted. Generally, the CVD method can be used to fabricate a uniform single-layer of nanosheets, because the atomic deposition process would dominate the transfer process in the whole fabrication process. On the other hand, sandwich structures of TMDs with single-layers and large-size sheets can also be prepared by CVD, such as the reaction of MoO_3 and S reactants at 650 °C on a SiO_2 substrate. However, due to the defects of the solid substrate and the presence of impurities, the preferential nucleation of microcrystals becomes an obstacle to limit the preparation of large-sized sheets by CVD. Recently, Chen *et al.*[43] successfully fabricated large-sized monolithic $MoSe_2$ using molten glass as the substrate. Fig. 2c shows the use of 20 sccm Ar as a carrier gas mixed with a small amount of H_2, and the MoO_3 reductant could control the starting and end points of the reaction. The CVD growth process was carried out at ambient pressure, and the growth of the selenium powder and the molten glass was maintained at 280 and 1050 °C, respectively. The glass substrate was placed in a quartz tube mounted in a tube furnace, and $MoSe_2$ was grown on the surface of the molten glass. It was obvious that $MoSe_2$ was deposited on the poly(methyl methacrylate) (PMMA) solid substrate, and the defects on the substrate led to this phenomenon. Different morphologies of the crystals decreased the size of the fabricated layer and increased the folding of the layer, which resulted in the formation of layers with larger surface area. These high-standard and large-sized TMD sheets prepared by CVD deposition and melting of the substrate have great potential for further applications.

2.2 Functionalization of TMD nanosheets for various applications

2.2.1 Ionic adsorption. There are special requirements for the preparation of TMD nanosheets in the biomedical field, particularly in the treatment of tumors. Researchers are interested in learning whether protein as a natural biopolymer contributes to the removal of TMD materials. If the protein can be used in auxiliary peeling and has an additional function of changing the lamellar surface, the field of medical nanomaterials will be expanded. Recently, Guan *et al.*[44] have successfully demonstrated that protein like bovine serum albumin (BSA) can indeed be used to prepare and modify 2D TMD nanosheets. The process of stripping different TMD materials (such as MoS_2, WS_2 and WSe_2) with BSA has also been reported by other groups.[45–47] Interestingly, BSA not only stripped MoS_2 nanosheets but also modified their surface properties. In addition, BSA can absorb toxic compounds and heavy metal ions. Therefore, BSA-modified MoS_2 sheets have shown the ability to absorb toxic substances and heavy metal ions, as shown in Fig. 3. At the same time, the strategy can be combined with PTT/PDT, considering that nanosheets can also absorb toxic substances that are produced during the tumor treatment. This functional approach has great potential in the medical field.

2.2.2 Temperature-resistant materials. TMD nanosheets can be used as photosensitizers for PTT.[48] In the preparation of TMD nanosheets, ultrasonic stripping methods have been widely used. Ultrasound can cause TMD nanosheets to rub against each other to release large amounts of heat, which may oxidize the TMD nanosheets. In this process light-heat conversion TMD nanosheets could obtain a lot of heat energy. Ordinary TMD nanosheets do not meet the needs of modern development, and therefore the development of high temperature-resistant TMD

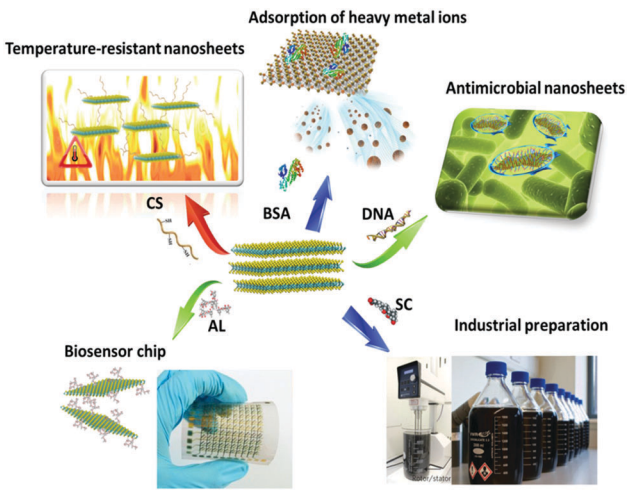

Fig. 3 The functionalization of TMD materials for various applications.

nanosheets has become important. Recently, Wang *et al.* used chitosan to elute MoS_2 nanosheets and studied the effect of CS on the temperature resistance of MoS_2.[49] It was found that CS would reduce the peak heat release of a MoS_2 sheet by 14.6%, so that the exotherm of MoS_2 was more gentle. This method relieves the oxidation of MoS_2 without affecting the photothermal conversion efficiency.[10] Several reports indicate that CS as a biological non-toxic material can be used for drug delivery. Therefore, the modification of TMD nanosheets by CS would largely favour the biomedical utilization of TMD materials in the fields of PTT and drug delivery.

2.2.3 Antimicrobial materials. Antibacterial materials have been one of the important research areas in the fields of biology and biomedicine. TMD nanosheets have also been used in the field of cancer treatment to meet the needs of high antibacterial capacity.[50] Pandit *et al.* modified MoS_2 nanosheets by using antimicrobial ligands.[51] Good antimicrobial effects were observed on two representative ESKAPE pathogenic strains of Gram-positive bacteria in the inhibition and sterilization of *Staphylococcus aureus* (MRSA) and Gram-negative copper-green pseudo-single bacteria (*Pseudomonas aeruginosa*). However, the synthesis of the antimicrobial ligands and the modification of the MoS_2 nanosheets were complex. In another study, Liu *et al.* prepared TMD nanosheets by stripping TMD nanosheets with DNA, which showed promising antibacterial activity (as shown in Fig. 3).[52] This study greatly simplified the preparation of antimicrobial TMD nanosheets. It is noteworthy that the DNA-assisted peeling and modification of the TMD surface effectively prevented the agglomeration of the nanosheets. In particular, the resulting WX_2–ssDNA nanosheets with less than 10 layers possess lateral dimensions of 65–650 nm. This method can be used to prepare monolayer or several-layer WX_2 nanosheets with good water dispersibility, as well as potent antimicrobial activity against *E. coli*, especially in the case of WSe_2–ssDNA nanoparticles (cell viability decreased by 82.3 ± 1.7%). This study on minimally invasive surgery is of great significance because it significantly reduced the possibility of infection.

2.2.4 Highly effective industrial materials. The high cost in the preparation of TMD nanosheets is an important problem in expanding their production.[53] Most TMD multilayered nanosheets have been centrifuged, either from top to bottom, or from bottom to top, resulting in a lower yield of nanosheets that cannot be produced on a large scale. Paton *et al.* used sodium cholesterate and NMP as surfactants to produce TMD nanosheets.[54] The TMD bulks were added to this mixed surfactant and then peeled off under shear force. Most of the prepared nanosheets were below 5 layers. This method effectively avoided material waste, making the industrialization of the preparation of TMD nanosheets possible.

2.2.5 Biosensors and biochips. The fabrication of both biosensors and biochips is a challenge in the field of smart wear. TMD materials have attracted much attention as a bio-non-toxic semiconductor material. However, the traditional peeling method cannot prepare TMD nanosheet dispersions with high concentration. Meanwhile, low concentration TMD nanosheet dispersions cannot be easily prepared for macroscopic bioelectronic components (Table 1).

Liu *et al.* used a lignin-assisted peeling method to successfully prepare MoS_2 nanosheet dispersions with a concentration greater than 10 mg mL^{-1}.[55] The prepared MoS_2 nanosheets had a thickness of 3.9 nm and a sheet size of 100 nm to 500 nm. Lignin as a natural biological macromolecule can effectively strip TMD nanosheets, and this non-toxic macromolecule can be used to prepare highly concentrated TMD nanosheet dispersions. In another study, a highly concentrated TMD dispersion has been obtained after putting a macro film through a simple filter, which showed promising applications for biosensing and biochips.[56,57]

3. Tumor imaging

3.1 CT imaging

X-ray CT imaging[20] is particularly important in medical applications. As the transition metal elements such as Mo and W are

Table 1 Various TMD materials with their applications and functions

Applications	Assisted molecule	2D material	Exfoliation method	Conc. (mg mL^{-1})	Function	Ref.
Adsorption	Bovine serum Albumin	MoS_2, WS_2, $MoSe_2$	Bath/tip sonication	0.3–6.8	Adsorption of heavy metal ions	44–47
PTT/PDT/drug delivery	Chitosan	MoS_2	Bath/tip sonication	1–5.4	High temperature, biocompatibility	10, 48, 49, 58 and 59
	PVP	$MoSe_2$	Bath/tip sonication	0.1	Nanosheets coated by polymer	60
	PLGA	MoS_2	Bath/tip sonication	—	Injection gel	61
Sensor/biochip	Lignin	MoS_2	Bath/tip sonication	0.62–12	High concentration	55–57
	Cellulose	MoS_2	Bath/tip sonication	0.2–0.7	Electrochemical performance	62–64
Antibacterial materials	DNA	MoS_2	Bath/tip sonication	0.5–2.3	Antibacterial	50, 52 and 65
	Thiol ligands	MoS_2	Butyllithium	1.6	Antibacterial	51
Mass production	Sodium cholate	MoS_2, $MoSe_2$, $MoTe_2$, WS_2, WSe_2, WTe_2, $NbSe_2$, $TaSe_2$	Shear mixing	0.8	Possibility of industrialization	53, 54 and 66
Imaging	PAA	MoS_2	Hydrothermal synthesis	0.2	Loading Gd for MR imaging	67 and 68
	$GdCl_3$	WS_2	Hydrothermal synthesis	2	Gd ion doping for MR imaging	69
	Bi_2S_3	MoS_2/Bi_2S_3	Hydrothermal synthesis	0.15	Composite nanosheets for CT/PA imaging	70
	mPEG-*co*-PPyr	MoS_2	Butyllithium	0.5	Shell structure for PA imaging	71

high atomic number elements, both MoS_2[72] and WS_2 can be used as CT contrast agents.[73] In order to improve the dispersibility of TMD nanosheets in blood, the general method is to modify the surface of the 2D TMD sheets with a hydrophilic polymer (*i.e.*, PEG, BSA).[74] The resulting modified 2D TMD materials are then more easily dispersed in the tumor site after being injected into the living body, which significantly improves the imaging quality. In addition, the HU (Heinz unit, which reflects the density of the substance) value of WS_2 is about 22.01 HU l g^{-1}, which is much higher than that of traditional iodopamine (14.76 HU l g^{-1}), suggesting its great potential for CT imaging applications. Compared with the rapid development of combined therapy, a single CT imaging contrast agent is unable to meet the needs of modern cancer treatment. CT imaging has been often used as a guide to assist PTT/PDT in the treatment of tumors. Therein, nanocomposites were followed by scanning in an XM-Tracer-130 CT imaging system, and the imaging effect of live CT is shown in Fig. 4a and b. This 2D TMD tumor treatment agent has the dual function of imaging and treatment. In the future, this kind of dual-functional nanomaterial will hopefully replace contrast agents with a single CT imaging function. In addition to the surface modification method, composite nanosheets can also be prepared by using a variety of functional CT contrast agents.

Recently, MoS_2/Bi_2S_3 composite nanosheets have been prepared *via* a hydrothermal reaction using $(NH_4)_2$ MoS_4 and $Bi(NO_3)_3$ by Wang *et al.*, particularly because Bi has good X-ray attenuation CT imaging properties.[70] Both Bi and Mo atoms in the composite lamellae are capable of attenuating X-rays, greatly increasing the stability and clarity of imaging. MoS_2 absorbed 808 nm NIR light and produced photothermal effects to kill cancer cells. The Bi atoms of the Bi_2S_3 lamellae showed a strong ability to absorb light under X-ray radiation and produced large amounts of short-range secondary electrons to enhance X-ray deposition in tumor tissue and accelerate DNA destruction. The fabricated composite nanosheets served dual functions for both bioimaging and therapy.

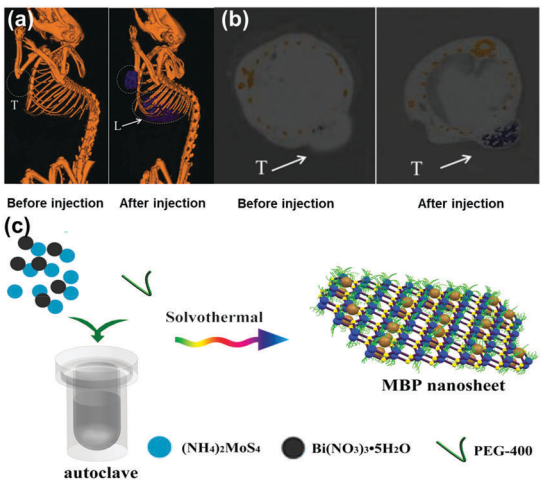

Fig. 4 (a) *In vivo* CT images of 4T1 tumor-bearing mice before and 6 h after intravenous injection of PEG–MoS_2–Au–Ce6 nanocomposites. (b) *In vivo* CT images of tumors in mice before and 6 h after intravenous injection of PEG–MoS_2–Au–Ce6 nanocomposites. Reprinted with permission from ref. 73. Copyright 2017 Royal Society of Chemistry. (c) Schematic illustration of solvothermal synthesis of MoS_2/Bi_2S_3 composite nanosheets. Reprinted with permission from ref. 70. Copyright 2015 Wiley-VCH.

3.2 MR imaging

MR imaging is a very significant imaging method in modern biomedical applications. To participate in MR imaging, TMD nanosheets (the surface or the middle layer of a TMD sandwich structure) should be first modified with some paramagnetic metal nanoparticles or ions. Recently, Cheng *et al.*[69] developed a bottom-up solution-phase method to synthesize WS_2 nanoflakes intrinsically doped with different types of metal ions (*e.g.*, Fe^{3+}, Co^{3+}, Ni^{2+}, Mn^{2+} and Gd^{3+}). They also chose Gd^{3+}-doped WS_2 (WS_2:Gd^{3+}) nanoflakes as a typical example to realize combined photothermal and radiation therapy under the guidance of trimodal imaging. As shown in Fig. 5,[69] first, the mixture of WCl_6 and MCl_x (M = Fe^{3+}, Co^{3+}, Ni^{2+}, Mn^{2+} and Gd^{3+}) at a certain proportion reacted in a mixed solvent of oleylamine (OM) and 1-octadecene at 300 °C under N_2 atmosphere. After completing the hydrothermal reaction, an intermediate complex was formed. Next, doped WS_2 nanosheets with paramagnetic metal ions were prepared by injecting a sulfur solution. In particular, NH_2–PEG was also introduced to modify the surface of the nanosheets to provide better dispersity in aqueous solution.

The WS_2 layer has the same sandwiched structure, but the number of W atoms in the interlayer of the sandwich layer was affected by the paramagnetic metal particles. The metal-ion doping ratios in the final products increased with the increase of added doping metal ions during the reaction. For example, the exact W : Gd ratio in the WS_2 : Gd^{3+} nanoflakes was 94.6 : 5.4 (WS_2 : Gd^{3+}), 86.7 : 13.3 (WS_2 : Gd^{3+}), and 84.3 : 15.7 (WS_2 : Gd^{3+}) for samples prepared with W : Gd feeding ratios of 90 : 10, 80 : 20, and 70 : 30, respectively. The corresponding samples were WS_2 : Gd^{3+}–1-PEG, WS_2 : Gd^{3+}–2-PEG and WS_2 : Gd^{3+}–3-PEG. The imaging effect is strongly dependent on the concentration of Gd^{3+} ions, as described in Fig. 6a.

As photothermal therapeutic agents, the paramagnetic metal-doped[76] WS_2 flakes were ideal candidates. Gd^{3+}-doped nanosheets had good near-infrared absorptivity in the spectral

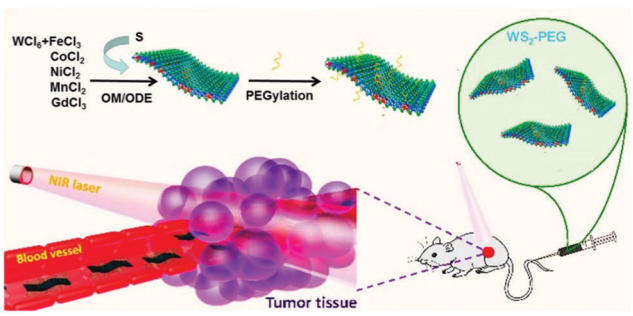

Fig. 5 Synthesis and composition analysis of WS_2:Mn_t (M = Fe^{3+}, Co^{2+}, Ni^{2+}, Mn^{2+}, and Gd^{3+}) nanoflakes prepared using a bottom-up method and injected into a tumor. Reprinted with permission from ref. 69. Copyright 2015 American Chemical Society.

range form 700–1000 nm comparable to a single WS_2 nanosheet. The mass extinction coefficient of a WS_2 nanosheet (22.6 l g^{-1} cm^{-1}) prepared using a hydrothermal method was slightly lower than that of the WS_2 nanosheet (23.8 l g^{-1} cm^{-1})[77] prepared using an exfoliation method, but it was much higher than that of graphene nanoplatelets (GO, 3.6 l g^{-1} cm^{-1}). Gd^{3+} ion concentration can affect the photothermal properties of nanosheets. The higher the Gd^{3+} ion concentration, the better the photothermal performance. As TMD materials can stabilize the doping of the metal ions in the nanosheet layer, they can be well used as a photothermal agent.

Unlike CT imaging with high atomic elements such as W and Mo, MR imaging is dependent on the TMD layer containing paramagnetic ions (*e.g.*, Fe^{3+}, Co^{3+}, Ni^{2+}, Mn^{2+} and Gd^{3+}) for contrast agent imaging. MR imaging does not require the use of ionizing radiation or the depth of penetration, making it an ideal approach for noninvasive longitudinal studies and as a powerful diagnostic tool for clinical and research purposes. Nuclear magnetic imaging has high spatial and temporal image resolution. On further combination with a magnetic field, ultra-high resolution can be achieved, making it particularly suitable for tumor imaging applications. The contrast of MR imaging is closely related to the quality of the contrast agent. As shown in Fig. 6b and c, different contrast agents can selectively shorten the longitudinal (T_1)[78] or transverse (T_2) relaxation time to expand the visualization range. Most MR imaging adopts a longitudinal (T_1) imaging mode. Gd^{3+} ions are one of the most widely used T_1 contrast agents due to the seven unpaired electrons (S = 7/2) of their outer layer and high magnetic moments. The limitation of using Gd^{3+} alone is that T_1 imaging is a low observed relaxation and eventually translates into signal ambiguity. The Gd^{3+} ions were then doped into the intermediate layer atoms of a TMD sheet, allowing the integration of MR with NIR imaging and CT imaging. MR provides detailed anatomical imaging, while NIR imaging provides high probe sensitivity for imaging molecular targets. The dual-modal imaging provided more accurate positioning of the photosensitizer and tumor location. This method was conducive to the next step in the cancer treatment, and light and heat provided by this process would play an important role in a combined treatment platform of tumors.

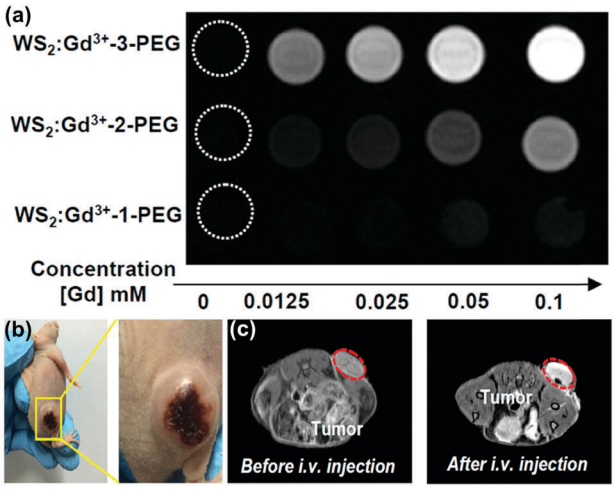

Fig. 6 (a) T_1-weighted MR images of WS_2:Gd^{3+}–PEG solutions with different concentrations. (b) Photographs of 4T1 tumor-bearing mice. Reprinted with permission from ref. 75. Copyright 2017 American Chemical Society. (c) T_1-weighted MR images of mice before and 24 h after i.v. injection of WS_2:Gd^{3+}–3-PEG (2 mg mL^{-1}, 200 μL). Reprinted with permission from ref. 69. Copyright 2015 American Chemical Society.

3.3 PA imaging

PA imaging is similar to conventional ultrasound imaging,[79] in which air microbubbles can improve the resolution of imaging. But ultrasound imaging is based on acoustic impedance changes when acoustic waves penetrate tumors. The ultrasonic agents around the air microbubbles will quickly disappear, which affects the performance of the ultrasound imaging.[80] Unlike ultrasound imaging, PA imaging utilizes the photothermal effect of TMD materials, which produce thermal signals by thermal expansion or bubble formation. Continuously created air microbubbles greatly improve the resolution of PA imaging. As an up-to-date imaging method, PA imaging has been the focus of application in bioelectromechanical interfaces.[81] As a rapidly growing technique with high contrast and large penetration depth, there is great potential for cancer molecular imaging. However, the molecular imaging of PA in brain tumors is still challenging, due to the lack of nanosheet sensitivity. Zheng *et al.* found that the thickness of the lamellae affected the absorption of NIR light, which indirectly affected the PA imaging effect.[82] Compared with few-layer (F-MoS_2) and multilayer MoS_2 (M-MoS_2), monolayer MoS_2 showed the best absorption of NIR and PA imaging sensitivity.

TMD nanocomposites have been studied in order to compensate the lack of PA imaging sensitivity. Recently, methoxyl-polyethylene glycol-*co*-pyrrole copolymer (mPEG-*co*-PPyr) nanoparticles (NPs) and mPEG-*co*-PPyrNP/MoS_2 were successfully prepared by Lee *et al.*[71] As shown in Fig. 7, both mPEG-*co*-PPyr NPs and mPEG-*co*-PPyr/MoS_2 nanocomposites exhibited PA signal activity, while MPEG-*co*-PPyr/MoS_2 nanocomposites exhibited higher PA signal amplitudes at 700 nm than mPEG-*co*-PPyr NPs. In that study, semiconducting polypyrrole was used as an electroactive material. PEG and MoS_2 nanosheets absorbed the heat energy that was released upon NIR light irradiation of TMD nanosheets, and converted it into an acoustic signal that can be used for PA imaging. This synergistic mode of NIR fluorescence imaging and PA compensated the drawback of NIR optical imaging. Due to the tissue penetration depth and spatial division of the uniform limit, the fluorescent polymer can be carried using the TMD nanosheets. These fluorescent polymers can be released inside the tumor. Different types of imaging modalities thus can be combined for tumor cells. Also, a nanosheet with a larger size could be used in drug loading and controlled release fields for combined treatment of tumors.

4. Tumor therapy

4.1 PTT

Optical therapy,[83] including PTT[84] and PDT,[8,85] has being a new generation of effective treatment of cancer featured by

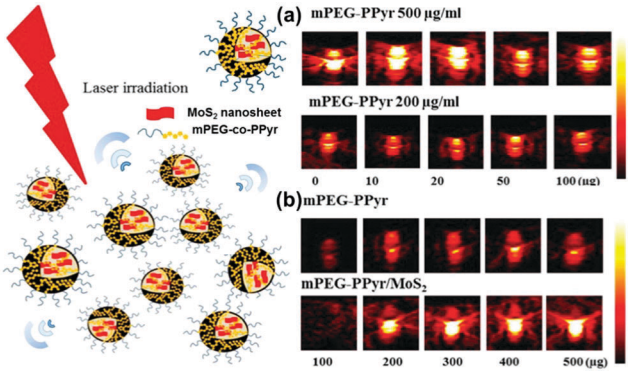

Fig. 7 Photoacoustic activity of mPEG-*co*-PPyr nanoparticles and mPEG-*co*-PPyr/MoS_2 nanocomposites. (a) PA signal of mPEG-*co*-PPyr/MoS_2 NCs with varied MoS_2 concentrations (0–100 μg), and (b) PA signal of mPEG-*co*-PPyr/MoS_2 NCs at constant MoS_2 concentration (20 μg) and with a varied concentration of mPEG-*co*-PPyr (100–500 μg). All mPEG-*co*-PPyr/MoS_2 NCs complexed with MoS_2 showed significantly enhanced photoacoustic activity. The average energy density of the laser irradiation was 14.48 mJ cm^{-2} in each experiment of (a) and (b). The inner and outer diameters of the used tygon tubes were ID 0.05 in, OD 0.09 in, and ID 0.04 in, OD 0.07 in, respectively, for experiments (a) and (b). Reprinted with permission from ref. 71. Copyright 2016 American Chemical Society.

minimally invasive therapy in recent years. Optical therapy exhibits rather weak side effects compared to traditional chemotherapy and radiotherapy, and the reagent preparation is simple and cheap. In particular, this treatment strategy can be applied for minimally invasive surgery with high flexibility. The core mechanism of PTT is the use of an appropriate photosensitizer dispersed in tumor cells, with strong tissue penetration of NIR light irradiation of tumors.[86] These photosensitizers can efficiently absorb NIR light and heat cells locally, which then warms up intracellular proteins and destroys tumor cells.

Recently, with the rapid development of nanotechnology, nanomaterial-based PTT has attracted more and more attention. Gold NPs and nanorods[87] have been used as photosensitizers in NIR therapy (*i.e.*, PTT). 1D carbon nanomaterials such as nanotubes have also been reported for use in PTT.[88] Since a single tumor therapy function no longer satisfies the clinical requirements, developing new, combined therapy approaches enabling two or even more therapies simultaneously is becoming necessary. 2D nanomaterials such as graphene could be used in biomedical PTT and controlled drug release. Combined treatment based on nanomaterials has already aroused a lot of attention from every corner of the world. Liquid-stripped TMD nanosheets have the advantages of high-yield, facile preparation and low cost. As the transition metal atoms have paramagnetism, they can be applied to preoperative CT, MR and PA imaging. TMD nanosheets with ultra-high surface area are capable of carrying small drugs and function as a postoperative drug delivery carrier. TMDs could become a photosensitizer due to their high light and heat conversion efficiency and stable chemical properties. In addition, the biological toxicity of some typical TMD materials like MoS_2, WS_2 and $MoSe_2$[89] could kill more than 90% of the tumor cells when used as a photosensitizer. Moreover, TMD materials can be harnessed as an essential intermediate link for PTT/bioimaging in a combined treatment platform.

Chou *et al.*[10] used a chemical stripping method to prepare amphiphilic MoS_2 for use in PTT. This amphiphilic MoS_2 layer ($ceMoS_2$) has a good aqueous dispersity compared to graphene nanosheets. The $ceMoS_2$ sheet has a size of 800 nm and a thickness of 1.54 nm. The NIR absorbance was 29.2 l g^{-1} cm^{-1}, higher than that of rGO nanosheets (24.6 l g^{-1} cm^{-1}), which was 7.8 times over the NIR absorbance of GO. Although MoS_2 nanosheets have not been used in combination therapy yet, it has been shown that TMD materials have great potential in phototherapy. Liu *et al.*[72] used iron oxide modified MoS_2 nanosheets and improved their hydrophilicity with PEG to develop a platform combining the photothermal function of TMD nanosheets and biological imaging (Fig. 8a). The volume of tumors was significantly reduced after 15 days of photothermal treatment following injection of MoS_2 lamellae-modified iron oxide composites into the mice (Fig. 8b). The measurement of the blood concentration of Mo by ICP-AES showed an MoS_2-IO-(d) PEG blood circulation half-life of 10 hours. The corresponding IR imaging indicated that the injection of MoS_2-IO-(d) PEG after 8 hours showed high performance for PTT imaging (Fig. 8c). In addition, the cell culture experiment indicated that the created PEG-modified MoS_2 has a good inhibitory effect on tumor cells (Fig. 8d). This study vividly illustrated the use of 2D-TMD materials for the construction of a multi-functional nanocomposite in multi-mode guided tumor therapy, demonstrating the great potential of two-dimensional TMD materials for combined treatment.

4.2 PDT

Different from PTT, PDT does not involve a heat conduction process,[90] and therefore the cancer cells around the healthy cells are not subject to heat transmission. PDT treatment typically uses 2D TMD lamellae carrying methylene blue (MB),[91] so by NIR light[92] illumination the formed $^1O_2$[93] will induce apoptosis of cells. Thus, in PDT treatment it is more important to ensure the precise localization of methylene blue in cancerous tumors, in order to avoid MB diffusing into the normal tissue cells and causing unnecessary apoptosis.[94]

Yong *et al.*[47] prepared BSA–WS_2@MB nanocomposites by MB loading with BSA-modified WS_2 nanolamellae for PTT–PDT co-treatment of tumor cells (Fig. 9a). They adopted H_2SO_4 intercalation ultrasonic stripping so that the obtained composites were not sensitive to water or air. Compared with the lithium ion intercalation approach, the yield using this method is higher, and the average thickness of the obtained WS_2 nanosheets was about 1.6 nm. With the BSA surface coating, the thickness of the WS_2 nanosheets increased to 4–5 nm, greatly improving the biocompatibility of the WS_2 lamellae and providing more binding sites for carrying MB (Fig. 9b). The WS_2–BSA@MB nanocomposites showed photothermal effects upon 808 nm NIR illumination. Within the cells, the temperature of the nanosheet layer increased and led to the release of MB molecules. The excitation wavelength of MB was 660 nm, so upon 660 nm NIR radiation free MB molecules released $^1O_2$ and

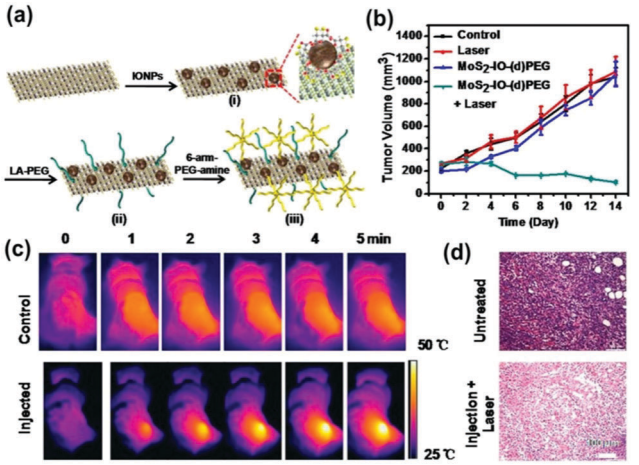

Fig. 8 (a) Schematic presentation to illustrate the self-assembly of DMSA-modified IONPs on exfoliated MoS_2 nanosheets and the subsequent PEGylation. (b) Tumor volume growth on mice (5 mice for each group) measured after various treatments indicated every 2 days for 2 weeks. (c) IR thermal images of 4T1 tumor-bearing mice without or with iv injection of MoS_2-IO-(d) PEG (dose of MoS_2 = 6.85 mg kg^{-1}) under 808 nm laser irradiation (0.78 W cm^{-2}) taken at different time intervals. The irradiation was conducted 8 h after injection. (d) H&E stained images of tumors sliced from an untreated mouse (upper) and a mouse 1 day after MoS_2-IO-(d) PEG-induced photothermal treatment. Reprinted with permission from ref. 72. Copyright 2015 American Chemical Society.

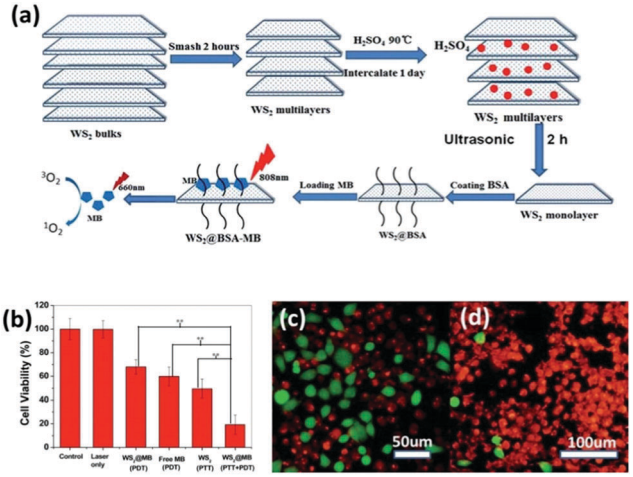

Fig. 9 (a) Schematic illustration of the synthetic procedure of WS_2 nanosheets and their application as a multifunctional photosensitizer delivery system for combined photothermal and photodynamic therapy of cancer. (b) *In vitro* cytotoxicity effect of PDT, PTT, and PTT + PDT. The output power of the 808 nm laser and 665 nm LED lamp for all tests was fixed at 1 W cm^{-2} for 15 min and 50 mW cm^{-2} for 5 min, respectively. Error bars were based on the standard deviation of six parallel samples. (c) Fluorescence images of HeLa cells incubated with WS_2 + 808 nm laser. (d) Fluorescence images of HeLa cells incubated with WS_2@MB + 808 nm laser + 665 nm LED. Green indicates live cells and red represents the dead ones. The concentration of WS_2@MB was fixed at 100 mg mL^{-1}. And the 808 nm laser (1 W cm^{-2}) and 665 nm LED (50 mW cm^{-2}) irradiation was carried out for 15 min and 5 min, respectively. Reprinted with permission from ref. 47. Copyright 2015 the Royal Society of Chemistry.

induced cancer cell apoptosis. The PTT and PDT dual synergistic therapy showed higher efficiency to kill the tumor cells. For example, the number of viable cells upon double treatment was significantly less than that subjected to single treatment, as shown in Fig. 9c and d. This is due to the fact that the MB molecules have not been absorbed from the WS_2 layer before absorbing NIR light excitation. If the MB molecules are free, the treatment will be more significant. It was found that under 808 nm and 660 nm dual NIR light irradiation, the majority of cells were killed. In contrast, many immunological cells still survived following irradiation with an 808 nm laser.

PTT/PDT is the main type of treatment in combined therapy platforms.[95] 2D TMD nanosheets as a key element for nanocomposites have an important position in the field of tumor therapy. On the basis of biomechanics and phototherapy, the use of ultra-high specific surface area combined with drug-loaded platforms has become a trend in the field of co-treatment.[96] At the same time developing more advanced platforms, for example, integrating imaging, light therapy and drug control in one material, is both an opportunity and a challenge.

4.3 NIR-controlled drug release

Drug delivery as a joint treatment platform for terminal systems has been booming since the 1960s, during which time controlled drug release technology has involved drug storage, drug implantation and drug injection. Drug-loaded platforms have gradually evolved from a functional polymer to nano-drug delivery, and then gradually to targeted drug release carriers. Modern medicine and cell biology have made great contributions to this field, and received widespread attention in tumor research. The role of drug-controlled release in combination with PTT is manifested in the recovery phase of PTT and PDT. Since the essence of PTT is the absorption of NIR heat thereby killing cancer cells,[97] the resultant high temperature may damage healthy cells around the tumors or increase the proliferation of tumor cells. In order to compensate the side effects of PTT, controlled drug release has been introduced as a terminal system in order to assist in the treatment to kill the residual tumor cells. Besides the capability of facilely controlling the release process, the carrier material itself should be biocompatible, non-toxic, and drug-resistant. The distribution of nanosheets affects the heat of directional conduction, and the dispersibility of the photothermal agent was also worthy of further exploration.[98] The emergence of 2D graphene sheet materials certainly led to the development of a drug delivery platform due to their high specific surface area and low toxicity.[99] However, a single drug-controlled carrier cannot meet the needs of combination therapy, and thus a variety of functional nanomaterial (such as TMD-based) carriers integrating bio-thermal imaging, PTT and controlled drug release capabilities have appeared for cancer treatment.

Drug-controlled carrier delivery response also requires the use of NIR excitation or temperature-sensitive stimulation.[100] Drug loading can be achieved, for example, by using materials from the traditional 2D layers through surface modification of thermo-sensitive macromolecules to the hydrogel system as the intermediate medium.[101] The purpose is to meet the needs of

different processes of tumor treatment, such as postoperative wound release and preoperative targeted delivery.

4.3.1 Hydrogel drug delivery for light therapy. Hydrogels have long been recognized in the field of biomaterials as smart materials.[102] Owing to their excellent biocompatibility and biodegradability, hydrogels have been widely used in biomedical repair materials.[103] For example, PINPAM hydrogel,[104] a thermo-sensitive material, has been widely used as a medical smart hydrogel.[105] The temperature variation will change the hydrophilicity of the polymer group, which then results in controlled release. Particularly, the drug release temperature of PINPAM hydrogels is close to the human body temperature. The combination of 2D nanomaterials with hydrogels has been successfully demonstrated in the case of graphene,[106] which has established the basis for the further application of TMD–polymer composites.

Recently, Lei *et al.*[107] prepared non-covalently modified hydrophilic $MoSe_2$ nanosheets by using polyvinylpyrrolidone (PVP) assisted peeling, and encapsulated them in PINPAM hydrogel. Based on this, they fabricated an intelligent drug delivery carrier platform with both light and thermal response capabilities (Fig. 10a). $MoSe_2$, as a member of the TMD family, has superior photothermal conversion efficiency. According to previous reports, the photothermal conversion efficiency (η) can be calculated based on eqn (1):[23]

$$\eta = \frac{h_S(T_{max} - T_{surr}) - Q_{Dis}}{I(1 - 10^{-A_{808}})} \quad (1)$$

The photothermal conversion efficiency of $MoSe_2$ was calculated to be 57.9%, which was much higher than that of Au nanorods (21%) and black phosphorus quantum dots (28.4%).[108,109] High thermal conversion efficiency suggested that $MoSe_2$ could be applied to a transdermal limited hydrogel system. It also favours the utility of hydrogel for drug loading and controlled release, that is, the drug release time is extended. The drug loading is independent of the $MoSe_2$ nanosheet and it is only related to the hydrogel system. The NIR-responsive, drug release-controlled hydrogel carrier does not have a targeting function, and the release of the drug is persistent and controllable. This hydrogel photothermal drug delivery system has been mainly used for wound repair and sterilization[110] or to kill residual tumor cells.

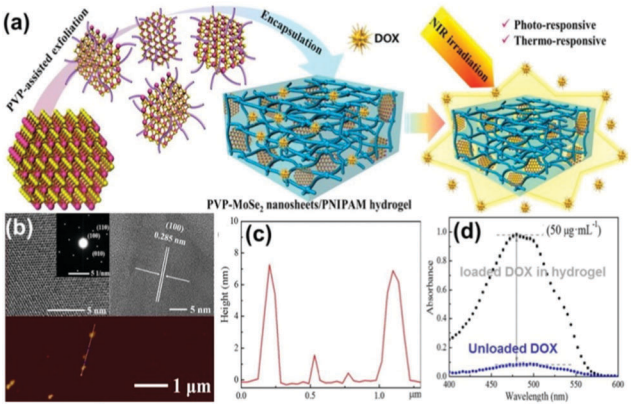

Fig. 10 (a) Scheme for preparation of PVP–$MoSe_2$ nanosheets/PNIPAM hydrogels. (b) Typical TEM and AFM images of $MoSe_2$ nanosheets, and (c) corresponding height profile. (d) UV-vis spectra of DOX encapsulation in nanocomposite hydrogels. Reprinted with permission from ref. 107. Copyright 2016 American Chemical Society.

This method used polymer-assisted peeling of the TMD material, and can yield functionalized 2D nanosheets using a one-step exfoliating modification process. Compared with conventional NMP-assisted liquid phase separation and a lithium ion insertion layer method, this polymer-assisted stripping process is simpler without the need of post-processing. Researchers found that (Fig. 10b and c) although the layer cannot be completely stripped as a single layer, the sheet itself has active functional groups without further modification. Moreover, no excess lithium ions or NMP molecules can be directly applied to the composite of bio-hydrogels, therefore, this method has a unique advantage in preparing biocompatible TMD nanomaterials.

PINPAM is known to undergo a significant reduction in volume when heated to the lower critical temperature, so upon NIR laser irradiation the size of the TMD–PINPAM hydrogel will also shrink due to the local heating. This NIR response of micro-brake intelligent materials[111] can be used to control drug release. The commonly-adopted strategy is using different heat-sensitive double hydrogels,[112] such as PNIPAM–DMA[25] composite hydrogels, where the PINPAM layer was doped into the TMD material, forming PINPAM-doped DMA hydrogels. Following the NIR light (808 nm) irradiation to the PINPAM layer,[113] the volume of the composites will shrink, but the DMA layer will not respond to temperature changes. It was observed that a double-layer composite gel will exhibit a certain curvature of bending, because the volume changes in the two kinds of hydrogel after heating would be different. This smart deformation material is not suitable for microscopic biomedical purposes owing to volume limitations, but it provides an innovative way to remotely control the shape of the deformed hydrogel. In addition, this hydrogel is non-toxic as a biological drug carrier. Fusco *et al.*[114] introduced a magnetic component (γ-Fe_2O_3) into double-layer hydrogels to develop a remote light-magnetically dual-controlled nano-robot for targeted drug release. Particularly, the effects of tubular hydrogels and tabular hydrogels on drug release were thoroughly evaluated, as shown in Fig. 11a and b. Further studies (Fig. 11c) revealed that the change in shape affects the release of the drug by the change in the surface area, and the drug release rate and amount by using the hollow tube was smaller than that of the tabular hydrogel. Thus it is possible to control the speed of drug release by remote light initiation or magnetic control of the shape of the drug carrier.

4.3.2 Surface functionalization of TMD nanosheets for drug loading. With the increase of 2D graphene and its wide use in sensing, catalysis,[115] electrochemical,[116] and other fields, the surface functionalization of 2D material surfaces for controlled drug release has also received intensive attention. Unlike the drug-loading mechanism of hydrogel systems, TMD drug carriers mainly rely on the ultra-high specific surface area of the 2D material itself, although they cannot achieve the ultra-high drug loading of a polymer system. However, analogous to other 2D materials, MoS_2 nanosheets showed higher

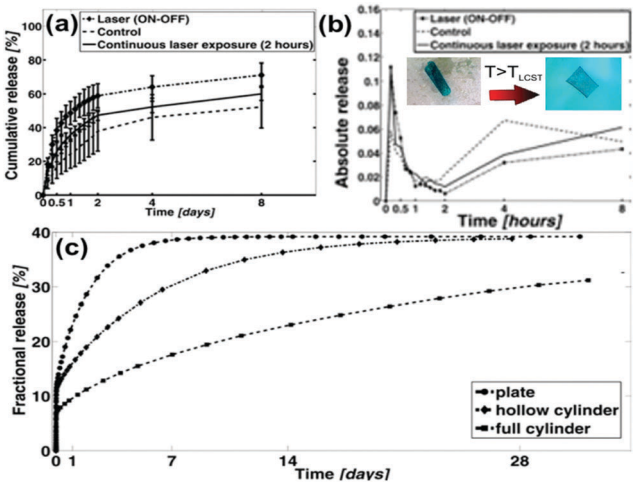

Fig. 11 (a and b) Cumulative release from morphing hydrogel microdevices. The light responsive bilayers unfold from a wrapped to an open square configuration, therefore increasing the surface area responsible for drug diffusion. Despite the contraction of the hydrogel, the general effect is a temporary increase of drug release upon unfolding. The process can be tuned by changing the exposure type and duration. (c) Curves of fractional release of the cylinder and plate, as simulated by the FEM diffusion driven model. A full cylinder with the same volume could achieve a much more linear, zero-order like profile over time. Reprinted with permission from ref. 114. Copyright 2015 American Chemical Society.

loading efficiencies for the control of drugs (doxorubicin, DOX), and the drug loading capacity of the MoS_2 nanosheet was 1.5 times that of graphene. PEG-modified TMD nanosheets have good biocompatibility and are uniformly dispersed in the blood,[117] facilitating the transport of the drug carrier through the blood circulation. They can also be more accurately administrated compared to hydrogel systems.

The release mechanism of 2D nanosheet-based drug carriers is the use of NIR light to irradiate the TMD nanosheets to produce photothermal effects. The heat is transferred along the surface of the nanosheets to a thermosensitive functional macromolecule, which is released afterwards. Sahoo *et al.*[118] reported a thermal transfer experiment of the lower MoS_2 prepared by CVD. The thermal conductivity of the 11-layer sample at room temperature was about 52 W m^{-1} K^{-1}. Fortunately, the TMD was a sandwich hexagonal structure, so the surface thermal conductivity of the TMD can be determined, unlike that of black phosphorus. Due to the presence of the trench structure, the surface heat transfer of the sheet surface has a different thermal conductivity along the transverse (perpendicular to the trench) and longitudinal (parallel to the trench) directions. Jain *et al.*[108] measured the thermal conductivity of black phosphorus at 300 K in the longitudinal and transverse directions, which was 110 W m^{-1} K^{-1} and 36 W m^{-1} K^{-1}, respectively. Thermal differences in different directions may lead to the release of drug-free molecules in a non-continuous manner. Compared to black phosphorus, the TMD material does not have a gully structure with the same heat transfer rate in different directions. Therefore, the temperature curve of TMD materials is continuous.

In addition to the specificity of TMD lamellae, surface modified co-functional polymers not only provided stronger drug delivery capacity, but also afforded nanocomposites with better biocompatibility and dispersibility. For instance, Yin *et al.*[119] coated MoS_2 nanoplates with modified chitosan (CS) and loaded them with anti-cancer drug DOX. The formed MoS_2–CS–DOX nanocomposites possess dual functions of PTT and drug controlled release. As shown in Fig. 12a, the method was a general approach of manufacturing drug cartridge shell structures, which can also be used in WS_2, $MoSe_2$, WSe_2 and other TMD nanosheets. Wang *et al.*[89] used the same method to coat poly-dopamine (PDA) during the hydrothermal synthesis of $MoSe_2$ nanolamellae. $MoSe_2$@PDA nanocomposites have been successfully prepared for drug loading and controlled release. In another work, MoS_2@CS has been prepared by the sonification of TMD nanosheets in the presence of sodium sulfate and CS in one step. CS is a commonly used linear biomaterial, and the original poor dispersion of the TMD layer in water was significantly improved upon CS modification. Even at a concentration up to 1 mg mL^{-1} in physiological solution, the MoS_2@CS can maintain a good dispersion for more than a week (Fig. 12b). In tumor cell therapy, DOX can be used as an effective drug for the treatment of tumors. As shown in Fig. 11c, the drug release rate in pH = 5 is highly sensitive to NIR light irradiation. The release rate was positively correlated with the increase of light power and heat density.

The development of TMD material-based systems capable of NIR absorption of light,[120] heat treatment, and lamellar light- or heat-induced release of DOX in cancer cells has been growing rapidly in recent years. Compared to a single drug treatment or the simple use of PTT, synergistic therapy could remove the tumor more efficiently. The side effects of organisms as shown by the changes in body weight of living mice reflect the health changes due to the presence of a drug action mechanism of PTT. The dual treatment system is more controllable than a mono-therapy system, and thus it can be selected for tumor cells to load and deliver different drugs. As reported by Ariyasu *et al.*,[121] MoS_2–CS loaded cyclic peptide sequence (cype) bound to intracellular heat shock protein (Hsp90). The inhibition of heat shock protein function would result in reduced heat resistance of cells. Therefore, cancer cells were killed under lower temperatures. The apparent advantage is that the damage to the surrounding healthy cells can be significantly reduced. Hsp90 is a protective companion protein biological system resistant to cell photothermal responses.[122] The inhibition of Hsp90 reduced the ability of cancer cells to resist PTT, allowing NIR to act on TMD lamellae. As a consequence, it is more likely to kill cancer cells and inhibit the transfer of cancer cells. The functionalized drug loading platform on the surface of the 2D TMD material is a modular nanocomposite drug delivery system, which can be loaded from selected drugs or polypeptides depending on the specific clinical requirements. Then the volume of tumor, tumor growth and weight change of mice were monitored through 15 days after injecting $MoSe_2$@PDA–DOX nanocomposites into mice, in order to compare the effect of combination therapy and monotherapy on tumors (Fig. 13a).

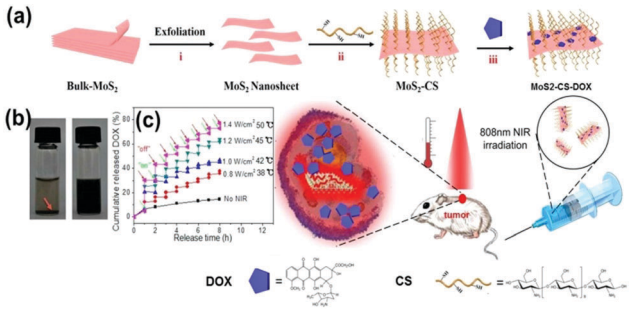

Fig. 12 (a) Schematic illustration of the high-throughput synthesis of MoS_2–CS nanosheets as an NIR photothermal triggered drug delivery system for efficient cancer therapy. Exfoliation process to produce single layer MoS_2 nanosheets which were then modified with CS, the DOX loading process, and NIR photothermal-triggered drug delivery of the MoS_2 nanosheets to the tumor site. (b) Digital photographs of the dispersion status of commercial MoS_2 flakes (left) and MoS_2–CS nanosheets (right) for at least 1 week. Concentration = 1 mg mL^{-1}. (c) Release profile of DOX in PBS buffer (pH 5.00) in the absence and presence of an 808 nm NIR laser. Reprinted with permission from ref. 119. Copyright 2014 American Chemical Society.

As it turned out, the tumor size of the mice injected with $MoSe_2$@PDA–DOX[89] was significantly smaller than that of the single use of $MoSe_2$@PDA for PTT or single injection of DOX drug therapy (Fig. 13b). Indeed, PTT ablated most of the tumor cells, but it was still less efficient compared with a dual combination therapy drug release material, $MoSe_2$@PDA–DOX. More importantly, to observe the weight of mice after injection, one can speculate that the release of drugs is conducive to reducing the negative effects of phototherapy on live tissue cells. This suggests that combination therapy is indeed feasible and has great potential for cancer treatment (Fig. 13c).

4.3.3 TMD nanosheets for targeted drug delivery. Targeted drug delivery is an important topic in the field of cancer therapy.[123] Targeted drug release includes active targeting and passive targeting. The active targeting refers to the ability to confer a drug or its vector to actively bind to a target. The primary principle includes the coupling of the probe molecule (antibody, polypeptide, sugar chain, nucleic acid aptamer) to the drug or its carrier surface by chemical or physical binding to achieve a targeted effect.[124] The passive targeting agents refer to the use of specific tissues and the physiological characteristics of organs. Therefore, the drugs in the human body can produce natural distribution differences. Due to the difference in the microvascular structure between solid tumors and normal tissues, the EPR effect can be used to achieve passive targeting.[125] For instance, Gao *et al.*[126] reviewed the wide applications of both active targeting and passive targeting in tumor therapy. Previously, quantum dots (QDs)[127] and polymer[128] based targeted drug deliveries have been reported. In this section, we focus on the applications of 2D TMD materials as vectors for targeted release of drugs.

It is well known that there are a number of defects on the surface of 2D TMD nanosheets, which provide a large number of active sites that are useful for functional surface modification with molecular probes. The conjugation of molecular probes onto TMD nanosheets created targeting functions for the final hybrid materials. For example, Zhang *et al.* modified MoS_2 nanosheets loaded with quantum dots by using an RGD (arginine-glycine-aspartic acid) probe for target drug delivery.[129] RGD has a specific recognition ability towards cervical cancer (HeLa) cells, and the fluorescent QDs show cell imaging function. Therefore, the use of RGD–QD–MoS_2 nanohybrids achieved triple targeting, imaging, and tumor therapy functions. Although this study did not involve drug release, it provided a potential way to modify TMD nanosheets with QDs and biological probes for targeted bioimaging and therapy.

The photosensitizer can also be used for target drug delivery. In this complex drug delivery system, the release of drugs

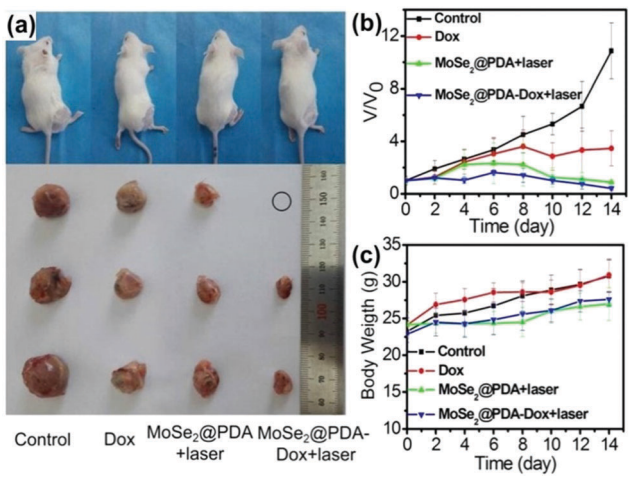

Fig. 13 (a) Representative photos of mice and tumors after various treatments. (b) Tumor growth curves of different groups after treatment. The tumor volumes were normalized by comparison with their initial sizes. (c) Mice weights of each group. Reprinted with permission from ref. 89. Copyright 2016 American Chemical Society.

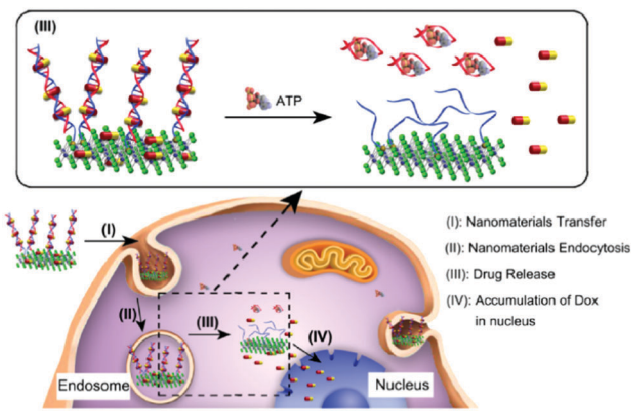

Fig. 14 Intracellular target drug delivery and chemotherapy with DNA-modified MoS_2 nanosheets. DNA oligonucleotides are used to modify MoS_2, and another complementary ssDNA ATP aptamer induces the formation of a DNA/MoS_2 superstucture. The addition of ATP into the DNA/MoS_2 system disassembles the multilayer superstructure and releases the drugs. Reproduced with permission from ref. 130. Copyright 2017 American Chemical Society.

is involved in a molecular dynamics process. In a typical study, Li and co-workers demonstrated the direct assembly and disassembly of 2D MoS_2 nanosheets with DNA for target drug delivery and chemotherapy, as shown in Fig. 14.[130] To achieve this aim, DNA oligonucleotides were firstly used to modify MoS_2 nanosheets and then the addition of another ssDNA ATP aptamer induced the formation of a multilayer DNA/MoS_2 superstructure. Therefore, the DOX drug could be bound to the MoS_2 surface and the DNA duplex *via* both physical and chemical interactions. The addition of ATP to this system resulted in the disassembly of this superstructure and the release of DOX to target cancer cell sites. The obtained results indicated that the carrier cells were swallowed by lysosomes and the presence of ATP molecules promoted the escape of DOX from lysosomes. The escaped DOX gathered in the nucleus and exhibited an excellent effect to kill cancer cells. For the first time, this study introduced an enhanced stimuli-responsive drug delivery system for targeted chemotherapy.

5. Conclusions and perspectives

In summary, 2D TMDs can be synthesized in large-scale production with facile approaches, and they possess exciting physicochemical properties comparable to graphene-based materials. The usage of polymer modification to prepare surface functionalized 2D TMD nanosheets has greatly simplified the preparation process and extended their potential applications. Furthermore, the high-yield preparation of TMD nanosheets is more suitable for future applications in biomedical fields, especially photo-treatment of cancer tissues. On the other hand, the sandwich structure of TMD materials provides stable chemical properties in which the transition metal layer doped paramagnetic particles can be applied to *in vivo* tumor imaging (CT, MR, PA imaging, fluorescent cell labelling). The bioimaging system can effectively detect the dispersibility of 2D TMD flakes (MoS_2, WS_2, and $MoSe_2$). TMD nanosheets as excellent drug nanocarriers can be combined with a hydrogel system to increase the performances of drug loading and release. It is also possible to utilize a thermo-sensitive deformable hydrogel to control the rate of release effectively, or deploy the lamellar surface modification function of the polymer to develop a targeted precision medical therapy. In addition, TMD nanosheets showed high biocompatibility and low cellular cytotoxicity, which are beneficial for their various biomedical applications. Compared to graphene-based materials, the sandwich structure of TMD materials made their chemical properties more stable, and therefore the reactivity with the chemical substances in the human body is lower than that of graphene. According to a previous study on the pharmacokinetics of TMDs, PEG-modified TMD nanosheets were excreted after 14 days, and there was no toxic physiological response in the test period.[72]

As the threat of cancer to humans has increased, the application of 2D TMD nanomaterials in biomedical fields has expanded rapidly. As a 2D TMD slice-based combination therapy platform, there is still a greater space for further development and improvement. Here we would like to present several insights and perspectives into this developing research field.

First, as the size and thickness of the TMD nanosheets cannot be effectively controlled by a top-down preparation method, it is necessary to develop novel, simple and high-yield preparation strategies of 2D TMD nanosheets with a uniform size and thickness. Second, the surface functionalization of TMD nanosheets with biomacromolecules, such as DNA, proteins, polypeptides, and others for cancer therapy should be investigated, which could enable the 2D TMD nanocarriers to possess specific cellular targeting and recognition functions. The directional binding of the drug carrier to the surface of the cell membrane remains a major challenge in the field of modern nano-drug delivery, thus the relevant progress will be much expected. Third, it will be valuable to evaluate the effects of local warming caused by TMD nanosheets on healthy cell tissues in the process of both photo- and heat-mediated therapy. 2D TMDs are injected into the inside of tumor tissues, and the location of the heat and the speed of warming are critical to the protection of the surrounding healthy tissue. Fourth, the accurate control and treatment of fever with 2D TMD nanosheet materials could be explored. As one of the combined treatment systems, light and heat therapy is used to inject photosensitizers into subcutaneous tumors to heat up tumor cells and to inactivate related proteins through photothermal effects. This method can be effective in the treatment of neoplastic diseases. However, the heat conduction will lead to the surrounding normal cell inactivation. Fifth, intelligent 2D TMD materials could be hopefully applied with either an electric field or a magnetic field to change the macroscopic orientation of nanosheets. In that way, the contact area between the lamellar and the linear light source, and also the heat conversion efficiency could be controlled to achieve precise treatment of the front tumors. An imaging tool can accurately show the dispersion uniformity of 2D nanosheets in a tumor center. The process is designed to ensure the effect of PTT/PDT to maximize the protection of surrounding normal tissue cells. Finally, multimodal treatments with electric field-, magnetic field-, photo-, and thermo-mediated therapies of cancers could be interesting. 2D TMD nanosheets have been used for combined therapy of tumors primarily *via* tumor imaging and PTT/PDT. This dual-modal therapy system has not yet tapped into the ideal potential of TMD materials.

We believe that this review will provide useful information and guidelines for readers and promote the exploration of the full potential of 2D TMD materials for biomedical applications.

Conflicts of interest

There are no conflicts to declare.

Acknowledgements

ZS gratefully acknowledges the financial support from the National Natural Science Foundation of China (NSFC, Grant No. 51573013).

Financial support from the National 1000 Young Talent Program (LS) and Program of Introducing Talents of Discipline to Universities (B08040) is also acknowledged. GW is thankful for the financial support from the Deutsche Forschungsgemeinschaft (DFG) under grants WE 5837/1-1.

References

1 Y. Chen, L. Cheng, Z. Dong, Y. Chao, H. Lei, H. Zhao, J. Wang and Z. Liu, *Angew. Chem., Int. Ed.*, 2017, **56**, 12991–12996.
2 F. Mao, L. Wen, C. Sun, S. Zhang, G. Wang, J. Zeng, Y. Wang, J. Ma, M. Gao and Z. Li, *ACS Nano*, 2016, **10**, 11145–11155.
3 J. Wang, X. Tan, X. Pang, L. Liu, F. Tan and N. Li, *ACS Appl. Mater. Interfaces*, 2016, **8**, 24331–24338.
4 M. Zhang, X. Zhao, G. Zhang, G. Wei and Z. Su, *J. Mater. Chem. B*, 2017, **5**, 1699–1711.
5 P. Zhang, X. Zhao, X. Zhang, Y. Lai, X. Wang, J. Li, G. Wei and Z. Su, *ACS Appl. Mater. Interfaces*, 2014, **6**, 7563–7571.
6 A. Gori, M. Cretich, R. Vanna, L. Sola, P. Gagni, G. Bruni, M. Liprino, F. Gramatica, S. Burastero and M. Chiari, *Anal. Chim. Acta*, 2017, **983**, 189–197.
7 W. Feng, L. Chen, M. Qin, X. Zhou, Q. Zhang, Y. Miao, K. Qiu, Y. Zhang and C. He, *Sci. Rep.*, 2015, **5**, 17422.
8 X. Yu, W. Zhang, P. Zhang and Z. Su, *Biosens. Bioelectron.*, 2017, **89**, 72–84.
9 Y. Li, P. Zhang, Z. Ouyang, M. Zhang, Z. Lin, J. Li, Z. Su and G. Wei, *Adv. Funct. Mater.*, 2016, **26**, 2122–2134.
10 S. S. Chou, B. Kaehr, J. Kim, B. M. Foley, M. De, P. E. Hopkins, J. Huang, C. J. Brinker and V. P. Dravid, *Angew. Chem.*, 2013, **52**, 4160–4164.
11 C. Chung, Y. K. Kim, D. Shin, S. R. Ryoo, B. H. Hong and D. H. Min, *Acc. Chem. Res.*, 2013, **46**, 2211–2224.
12 Y. Chen, C. L. Tan, H. Zhang and L. Z. Wang, *Chem. Soc. Rev.*, 2015, **44**, 2681–2701.
13 P. P. Zhang, X. Y. Lu, Y. Huang, J. W. Deng, L. Zhang, F. Ding, Z. Q. Su, G. Wei and O. G. Schmidt, *J. Mater. Chem. A*, 2015, **3**, 14562–14566.
14 X. N. Zhao, Y. Li, Y. Q. Guo, Y. J. Chen, Z. Q. Su and P. P. Zhang, *Adv. Mater. Interfaces*, 2016, **3**, 2196–7350.
15 D. M. Lin, Y. Li, P. P. Zhang, W. S. Zhang, J. W. Ding, J. F. Li, G. Wei and Z. Q. Su, *RSC Adv.*, 2016, **6**, 52739–52745.
16 Y. L. Xu, X. Y. Niu, H. L. Chen, S. G. Zhao and X. G. Chen, *Chin. Chem. Lett.*, 2017, **28**, 338–344.
17 X. Z. Cui, Z. G. Zhou, Y. Yang, J. Wei, J. Wang, M. W. Wang, H. Yang, Y. J. Zhang and S. P. Yang, *Chin. Chem. Lett.*, 2015, **26**, 749–754.
18 A. F. Rigos, H. M. Hill, Y. L. Li, A. Chernikov and T. F. Heinz, *Nano Lett.*, 2015, **15**, 5033–5038.
19 P. Shah, T. N. Narayanan, C. Z. Li and S. Alwarappan, *Nanotechnology*, 2015, **26**, 31.
20 Y. Y. Cui, J. Yang, Q. F. Zhou, P. Liang, Y. L. Wang, X. Y. Gao and Y. T. Wang, *ACS Appl. Mater. Interfaces*, 2017, **9**, 5900–5906.
21 W. J. Sun, S. Thies, J. L. Zhang, C. Peng, G. Y. Tang, M. W. Shen, A. Pich and X. Y. Shi, *ACS Appl. Mater. Interfaces*, 2017, **9**, 3411–3418.
22 K. Y. Pu, A. J. Shuhendler, J. V. Jokerst, J. G. Mei, S. S. Gambhir, Z. N. Bao and J. H. Rao, *Nat. Nanotechnol.*, 2014, **9**, 233–239.
23 Z. Y. Lei, W. C. Zhu, S. J. Xu, J. Ding, J. X. Wan and P. Y. Wu, *ACS Appl. Mater. Interfaces*, 2016, **8**, 20900–20908.
24 D. Zhang, M. Wu, Y. Zeng, L. Wu, Q. Wang, X. Han, X. Liu and J. Liu, *ACS Appl. Mater. Interfaces*, 2015, **7**, 8176–8187.
25 Z. Y. Lei, W. C. Zhu, S. T. Sun and P. Y. Wu, *Nanoscale*, 2016, **8**, 18800–18807.
26 W. Liu, W. S. Zhang, X. Q. Yu, G. H. Zhang and Z. Q. Su, *Polym. Chem.*, 2016, **7**, 5749–5762.
27 Y. H. Lee, X. Q. Zhang, W. Zhang, M. T. Chang, C. T. Lin, K. D. Chang, Y. C. Yu, J. T. Wang, C. S. Chang, L. J. Li and T. W. Lin, *Adv. Mater.*, 2012, **24**, 2320–2325.
28 D. Z. Zhang, Y. E. Sun, P. Li and Y. Zhang, *ACS Appl. Mater. Interfaces*, 2016, **8**, 14142–14149.
29 X. Li, J. Y. Shan, W. Z. Zhang, S. Su, L. H. Yuwen and L. H. Wang, *Small*, 2017, **13**, 1602660.
30 M. Chhowalla, Z. F. Liu and H. Zhang, *Chem. Soc. Rev.*, 2015, **44**, 2584–2586.
31 Z. B. Li and S. L. Wong, *Mater. Sci. Eng., C*, 2017, **70**, 1095–1106.
32 D. Chimene, D. L. Alge and A. K. Gaharwar, *Adv. Mater.*, 2015, **27**, 7261–7284.
33 J. Xia, X. Huang, L.-Z. Liu, M. Wang, L. Wang, B. Huang, D.-D. Zhu, J.-J. Li, C.-Z. Gu and X.-M. Meng, *Nanoscale*, 2014, **6**, 8949.
34 K. S. Novoselov, D. Jiang, F. Schedin, T. J. Booth, V. V. Khotkevich, S. V. Morozov and A. K. Geim, *Proc. Natl. Acad. Sci. U. S. A.*, 2005, **102**, 10451–10453.
35 T. Xing, S. Mateti, L. H. Li, F. X. Ma, A. J. Du, Y. Gogotsi and Y. Chen, *Sci. Rep.*, 2016, **6**, 35532.
36 Z. Y. Zeng, Z. Y. Yin, X. Huang, H. Li, Q. Y. He, G. Lu, F. Boey and H. Zhang, *Angew. Chem.*, 2011, **50**, 11093–11097.
37 X. B. Fan, P. T. Xu, Y. C. Li, D. K. Zhou, Y. F. Sun, M. A. T. Nguyen, M. Terrones and T. E. Mallouk, *J. Am. Chem. Soc.*, 2016, **138**, 5143–5149.
38 X. B. Fan, P. T. Xu, D. K. Zhou, Y. F. Sun, Y. G. C. Li, M. A. T. Nguyen, M. Terrones and T. E. Mallouk, *Nano Lett.*, 2015, **15**, 5956–5960.
39 C. Backes, R. J. Smith, N. McEvoy, N. C. Berner, D. McCloskey, H. C. Nerl, A. O'Neill, P. J. King, T. Higgins, D. Hanlon, N. Scheuschner, J. Maultzsch, L. Houben, G. S. Duesberg, J. F. Donegan, V. Nicolosi and J. N. Coleman, *Nat. Commun.*, 2014, **5**, 4576.
40 J. F. Shen, Y. M. He, J. J. Wu, C. T. Gao, K. Keyshar, X. Zhang, Y. C. Yang, M. X. Ye, R. Vajtai, J. Lou and P. M. Ajayan, *Nano Lett.*, 2015, **15**, 5449–5454.
41 V. Sreshtt, A. A. H. Padua and D. Blankschtein, *ACS Nano*, 2015, **9**, 8255–8268.
42 C. L. Tan and H. Zhang, *J. Am. Chem. Soc.*, 2015, **137**, 12162–12174.
43 J. Y. Chen, X. X. Zhao, S. J. R. Tan, H. Xu, B. Wu, B. Liu, D. Y. Fu, W. Fu, D. C. Geng, Y. P. Liu, W. Liu, W. Tang,

L. J. Li, W. Zhou, T. C. Sum and K. P. Loh, *J. Am. Chem. Soc.*, 2017, **139**, 1073–1076.
44 G. Guan, S. Zhang, S. Liu, Y. Cai, M. Low, C. P. Teng, I. Y. Phang, Y. Cheng, K. L. Duei, B. M. Srinivasan, Y. Zheng, Y. W. Zhang and M. Y. Han, *J. Am. Chem. Soc.*, 2015, **137**, 6152–6155.
45 S. Ahadian, M. Estili, V. J. Surya, J. Ramon-Azcon, X. Liang, H. Shiku, M. Ramalingam, T. Matsue, Y. Sakka, H. Bae, K. Nakajima, Y. Kawazoe and A. Khademhosseini, *Nanoscale*, 2015, **7**, 6436–6443.
46 A. Pattammattel and C. V. Kumar, *Adv. Funct. Mater.*, 2015, **25**, 7088–7098.
47 Y. Yong, L. Zhou, Z. Gu, L. Yan, G. Tian, X. Zheng, X. Liu, X. Zhang, J. Shi, W. Cong, W. Yin and Y. Zhao, *Nanoscale*, 2014, **6**, 10394–10403.
48 I. Uysal Unalan, C. Wan, S. Trabattoni, L. Piergiovanni and S. Farris, *RSC Adv.*, 2015, **5**, 26482–26490.
49 D. Wang, L. Song, K. Zhou, X. Yu, Y. Hu and J. Wang, *J. Mater. Chem. A*, 2015, **3**, 14307–14317.
50 G. S. Bang, S. Cho, N. Son, G. W. Shim, B. K. Cho and S. Y. Choi, *ACS Appl. Mater. Interfaces*, 2016, **8**, 1943–1950.
51 S. Pandit, S. Karunakaran, S. K. Boda, B. Basu and M. De, *ACS Appl. Mater. Interfaces*, 2016, **8**, 31567–31573.
52 F. Liu, J. Y. Choi and T. S. Seo, *Chem. Commun.*, 2010, **46**, 2844–2846.
53 R. J. Smith, P. J. King, M. Lotya, C. Wirtz, U. Khan, S. De, A. O'Neill, G. S. Duesberg, J. C. Grunlan, G. Moriarty, J. Chen, J. Wang, A. I. Minett, V. Nicolosi and J. N. Coleman, *Adv. Mater.*, 2011, **23**, 3944–3948.
54 K. R. Paton, E. Varrla, C. Backes, R. J. Smith, U. Khan, A. O'Neill, C. Boland, M. Lotya, O. M. Istrate, P. King, T. Higgins, S. Barwich, P. May, P. Puczkarski, I. Ahmed, M. Moebius, H. Pettersson, E. Long, J. Coelho, S. E. O'Brien, E. K. McGuire, B. M. Sanchez, G. S. Duesberg, N. McEvoy, T. J. Pennycook, C. Downing, A. Crossley, V. Nicolosi and J. N. Coleman, *Nat. Mater.*, 2014, **13**, 624–630.
55 W. Liu, C. Zhao, R. Zhou, D. Zhou, Z. Liu and X. Lu, *Nanoscale*, 2015, **7**, 9919–9926.
56 W. Liu, R. Zhou, D. Zhou, G. Ding, J. M. Soah, C. Y. Yue and X. Lu, *Carbon*, 2015, **83**, 188–197.
57 H. Lou, D. Zhu, L. Yuan, X. Qiu, X. Lin, D. Yang and Y. Li, *J. Phys. Chem. C*, 2015, **119**, 23221–23230.
58 X. Feng, X. Wang, W. Xing, K. Zhou, L. Song and Y. Hu, *Compos. Sci. Technol.*, 2014, **93**, 76–82.
59 W. Zhang, Y. Wang, D. Zhang, S. Yu, W. Zhu, J. Wang, F. Zheng, S. Wang and J. Wang, *Nanoscale*, 2015, **7**, 10210–10217.
60 A. B. Bourlinos, V. Georgakilas, R. Zboril, T. A. Steriotis, A. K. Stubos and C. Trapalis, *Solid State Commun.*, 2009, **149**, 2172–2176.
61 S. Wang, Y. Chen, X. Li, W. Gao, L. Zhang, J. Liu, Y. Zheng, H. Chen and J. Shi, *Adv. Mater.*, 2015, **27**, 7117–7122.
62 P. M. Carrasco, S. Montes, I. García, M. Borghei, H. Jiang, I. Odriozola, G. Cabañero and V. Ruiz, *Carbon*, 2014, **70**, 157–163.
63 Y. Li, H. Zhu, F. Shen, J. Wan, S. Lacey, Z. Fang, H. Dai and L. Hu, *Nano Energy*, 2015, **13**, 346–354.
64 J. M. Malho, P. Laaksonen, A. Walther, O. Ikkala and M. B. Linder, *Biomacromolecules*, 2012, **13**, 1093–1099.
65 D. Joseph, S. Seo, D. R. Williams and K. E. Geckeler, *ACS Appl. Mater. Interfaces*, 2014, **6**, 3347–3356.
66 S. De, P. J. King, M. Lotya, A. O'Neill, E. M. Doherty, Y. Hernandez, G. S. Duesberg and J. N. Coleman, *Small*, 2010, **6**, 458–464.
67 L. Chen, Y. Feng, X. Zhou, Q. Zhang, W. Nie, W. Wang, Y. Zhang and C. He, *ACS Appl. Mater. Interfaces*, 2017, **9**, 17347–17358.
68 L. Chen, X. Zhou, W. Nie, W. Feng, Q. Zhang, W. Wang, Y. Zhang, Z. Chen, P. Huang and C. He, *ACS Appl. Mater. Interfaces*, 2017, **9**, 17786–17798.
69 L. Cheng, C. Yuan, S. Shen, X. Yi, H. Gong, K. Yang and Z. Liu, *ACS Nano*, 2015, **9**, 11090–11101.
70 S. Wang, X. Li, Y. Chen, X. Cai, H. Yao, W. Gao, Y. Zheng, X. An, J. Shi and H. Chen, *Adv. Mater.*, 2015, **27**, 2775–2782.
71 H. Lee, H. Kim, T. P. Nguyen, J. H. Chang, S. Y. Kim, H. Kim and E. Kang, *ACS Appl. Mater. Interfaces*, 2016, **8**, 29213–29219.
72 T. Liu, S. X. Shi, C. Liang, S. D. Shen, L. Cheng, C. Wang, X. J. Song, S. Goel, T. E. Barnhart, W. B. Cai and Z. Liu, *ACS Nano*, 2015, **9**, 950–960.
73 L. Liu, J. P. Wang, X. X. Tan, X. J. Pang, Q. You, Q. Sun, F. P. Tan and N. Li, *J. Mater. Chem. B*, 2017, **5**, 2286–2296.
74 L. Cheng, J. Liu, X. Gu, H. Gong, X. Shi, T. Liu, C. Wang, X. Wang, G. Liu, H. Xing, W. Bu, B. Sun and Z. Liu, *Adv. Mater.*, 2014, **26**, 1886–1893.
75 H. Lin, X. G. Wang, L. D. Yu, Y. Chen and J. L. Shi, *Nano Lett.*, 2017, **17**, 384–391.
76 J. Kern, A. Trugler, I. Niehues, J. Ewering, R. Schmidt, R. Schneider, S. Najmaei, A. George, J. Zhang, J. Lou, U. Hohenester, S. M. de Vasconcellos and R. Bratschitscht, *ACS Photonics*, 2015, **2**, 1260–1265.
77 G. B. Yang, H. Gong, T. Liu, X. Q. Sun, L. Cheng and Z. Liu, *Biomaterials*, 2015, **60**, 62–71.
78 S. Y. Zhou, Z. K. Wu, X. S. Chen, L. S. Jia and W. Zhu, *ACS Appl. Mater. Interfaces*, 2014, **6**, 11459–11469.
79 E. Pisani, N. Tsapis, J. Paris, V. Nicolas, L. Cattel and E. Fattal, *Langmuir*, 2006, **22**, 4397–4402.
80 Y. R. Huang, A. M. Vezeridis, J. Wang, Z. Wang, M. Thompson, R. F. Mattrey and N. C. Gianneschi, *J. Am. Chem. Soc.*, 2017, **139**, 15–18.
81 A. Dragulescu-Andrasi, S. R. Kothapalli, G. A. Tikhomirov, J. H. Rao and S. S. Gambhir, *J. Am. Chem. Soc.*, 2013, **135**, 11015–11022.
82 J. Chen, C. Liu, D. Hu, F. Wang, H. Wu, X. Gong, X. Liu, L. Song, Z. Sheng and H. Zheng, *Adv. Funct. Mater.*, 2016, **26**, 8715–8725.
83 J. T. Robinson, S. M. Tabakman, Y. Y. Liang, H. L. Wang, H. S. Casalongue, D. Vinh and H. J. Dai, *J. Am. Chem. Soc.*, 2011, **133**, 6825–6831.
84 C. Liang, S. Diao, C. Wang, H. Gong, T. Liu, G. S. Hong, X. Z. Shi, H. J. Dai and Z. Liu, *Adv. Mater.*, 2014, **26**, 5646–5652.

85 R. C. Lv, D. Yang, P. P. Yang, J. T. Xu, F. He, S. L. Gai, C. X. Li, Y. L. Dai, G. X. Yang and J. Lin, *Chem. Mater.*, 2016, **28**, 4724–4734.
86 Z. Q. Meng, F. Wei, R. H. Wang, M. G. Xia, Z. G. Chen, H. P. Wang and M. F. Zhu, *Adv. Mater.*, 2016, **28**, 245–253.
87 M. Cheng, H. R. Wang, Z. Zhang, N. Li, X. H. Fang and S. S. Xu, *ACS Appl. Mater. Interfaces*, 2014, **6**, 1569–1575.
88 Z. Zhu, Z. W. Tang, J. A. Phillips, R. H. Yang, H. Wang and W. H. Tan, *J. Am. Chem. Soc.*, 2008, **130**, 10856–10857.
89 C. Wang, J. Bai, Y. Liu, X. Jia and X. Jiang, *ACS Biomater. Sci. Eng.*, 2016, **2**, 2011–2017.
90 C. S. Kue, A. Kamkaew, H. B. Lee, L. Y. Chung, L. V. Kiew and K. Burgess, *Mol. Pharmaceutics*, 2015, **12**, 212–222.
91 M. V. Junqueira, F. B. Borghi-Pangoni, S. B. S. Ferreira, B. R. Rabello, N. Hioka and M. L. Bruschi, *Langmuir*, 2016, **32**, 19–27.
92 M. Gonzalez-Bejar, P. Montes-Navajas, H. Garcia and J. C. Scaiano, *Langmuir*, 2009, **25**, 10490–10494.
93 Y. Tang, H. B. Chen, K. W. Chang, Z. H. Liu, Y. Wang, S. N. Qu, H. Xu and C. F. Wu, *ACS Appl. Mater. Interfaces*, 2017, **9**, 3419–3431.
94 T. Y. Wang, M. D. J. Libardo, A. M. Angeles-Boza and J. P. Pellois, *ACS Chem. Biol.*, 2017, **12**, 1170–1182.
95 S. W. Wang, X. Y. Zhao, S. C. Wang, J. Qian and S. L. He, *ACS Appl. Mater. Interfaces*, 2016, **8**, 24368–24384.
96 J. Wang, G. Z. Zhu, M. X. You, E. Q. Song, M. I. Shukoor, K. J. Zhang, M. B. Altman, Y. Chen, Z. Zhu, C. Z. Huang and W. H. Tan, *ACS Nano*, 2012, **6**, 5070–5077.
97 Y. X. Wang, N. Xu, D. Y. Li and J. Zhu, *Adv. Funct. Mater.*, 2017, **27**, 1604134.
98 J. I. Paredes, J. M. Munuera, S. Villar-Rodil, L. Guardia, M. Ayan-Varela, A. Pagan, S. D. Aznar-Cervantes, J. L. Cenis, A. Martinez-Alonso and J. M. D. Tascon, *ACS Appl. Mater. Interfaces*, 2016, **8**, 27974–27986.
99 L. H. Shao, R. R. Zhang, J. Q. Lu, C. Y. Zhao, X. W. Deng and Y. Wu, *ACS Appl. Mater. Interfaces*, 2017, **9**, 1226–1236.
100 C. Yao, P. Y. Wang, X. M. Li, X. Y. Hu, J. L. Hou, L. Y. Wang and F. Zhang, *Adv. Mater.*, 2016, **28**, 9341–9348.
101 Y. Toumia, S. Orlanducci, F. Basoli, S. Licoccia and G. Paradossi, *J. Phys. Chem. B*, 2015, **119**, 2051–2061.
102 X. Dong, C. Wei, H. L. Chen, J. W. Qin, J. Liang, D. L. Kong, T. J. Liu and F. Lv, *ACS Biomater. Sci. Eng.*, 2016, **2**, 2001–2010.
103 J. Liu, C. Qi, K. X. Tao, J. X. Zhang, J. Zhang, L. M. Xu, X. L. Jiang, Y. T. Zhang, L. Huang, Q. L. Li, H. J. Xie, J. B. Gao, X. M. Shuai, G. B. Wang, Z. Wang and L. Wang, *ACS Appl. Mater. Interfaces*, 2016, **8**, 6411–6422.
104 L. Han, Y. N. Zhang, X. Lu, K. F. Wang, Z. M. Wang and H. P. Zhang, *ACS Appl. Mater. Interfaces*, 2016, **8**, 29088–29100.
105 Z. M. Fang, G. X. Bai, W. T. Huang, Z. X. Wang, X. L. Wang and M. Y. Zhang, *Front. Plant Sci.*, 2017, **8**, 1338.
106 A. Paul, A. Hasan, H. Al Kindi, A. K. Gaharwar, V. T. S. Rao, M. Nikkhah, S. R. Shin, D. Krafft, M. R. Dokmeci, D. Shum-Tim and A. Khademhosseini, *ACS Nano*, 2014, **8**, 8050–8062.
107 Z. Y. Lei, Y. Y. Zhou and P. Y. Wu, *Small*, 2016, **12**, 3112–3118.
108 A. Jain and A. J. H. McGaughey, *Sci. Rep.*, 2015, **5**, 8501.
109 Z. B. Sun, H. H. Xie, S. Y. Tang, X. F. Yu, Z. N. Guo, J. D. Shao, H. Zhang, H. Huang, H. Y. Wang and P. K. Chu, *Angew. Chem., Int. Ed.*, 2015, **54**, 11526–11530.
110 T. I. Kim, B. Kwon, J. Yoon, I. J. Park, G. S. Bang, Y. Park, Y. S. Seo and S. Y. Choi, *ACS Appl. Mater. Interfaces*, 2017, **9**, 7908–7917.
111 K. Shi, Z. Liu, Y. Y. Wei, W. Wang, X. J. Ju, R. Xie and L. Y. Chu, *ACS Appl. Mater. Interfaces*, 2015, **7**, 27289–27298.
112 Y. Zhou, A. W. Hauser, N. P. Bende, M. G. Kuzyk and R. C. Hayward, *Adv. Funct. Mater.*, 2016, **26**, 5447–5452.
113 J. H. Huang, L. Zhao, T. Wang, W. X. Sun and Z. Tong, *ACS Appl. Mater. Interfaces*, 2016, **8**, 12384–12392.
114 S. Fusco, H. W. Huang, K. E. Peyer, C. Peters, M. Haberli, A. Ulbers, A. Spyrogianni, E. Pellicer, J. Sort, S. E. Pratsinis, B. J. Nelson, M. S. Sakar and S. Pane, *ACS Appl. Mater. Interfaces*, 2015, **7**, 6803–6811.
115 W. Y. Yin, J. Yu, F. T. Lv, L. Yan, L. R. Zheng, Z. J. Gu and Y. L. Zhao, *ACS Nano*, 2016, **10**, 11000–11011.
116 X. Y. Yu, M. S. Prevot and K. Sivula, *Chem. Mater.*, 2014, **26**, 5892–5899.
117 J. H. Appel, D. O. Li, J. D. Podlevsky, A. Debnath, A. A. Green, Q. H. Wang and J. Chae, *ACS Biomater. Sci. Eng.*, 2016, **2**, 361–367.
118 S. Sahoo, A. P. S. Gaur, M. Ahmadi, M. J. F. Guinel and R. S. Katiyar, *J. Phys. Chem. C*, 2013, **117**, 9042–9047.
119 W. Y. Yin, L. Yan, J. Yu, G. Tian, L. J. Zhou, X. P. Zheng, X. Zhang, Y. Yong, J. Li, Z. J. Gu and Y. L. Zhao, *ACS Nano*, 2014, **8**, 6922–6933.
120 J.-X. Fan, M.-D. Liu, C.-X. Li, S. Hong, D.-W. Zheng, X.-H. Liu, S. Chen, H. Cheng and X.-Z. Zhang, *Nanoscale Horiz.*, 2017, **2**, 349–355.
121 S. Ariyasu, J. Mu, X. Zhang, Y. Huang, E. K. L. Yeow, H. Zhang and B. G. Xing, *Bioconjugate Chem.*, 2017, **28**, 1059–1067.
122 Y. Y. Li, T. Zhang, Y. Q. Jiang, H. F. Lee, S. J. Schwartz and D. X. Sun, *Mol. Pharmaceutics*, 2009, **6**, 1152–1159.
123 W. Zhao, A. H. Li, C. Chen, F. Y. Quan, L. Sun, A. T. Zhang, Y. W. Zheng and J. Q. Liu, *J. Mater. Chem. B*, 2017, **5**, 7403–7414.
124 A. Lamprecht, N. Ubrich, H. Yamamoto, U. Schafer, H. Takeuchi, P. Maincent, Y. Kawashima and C. M. Lehr, *J. Pharmacol. Exp. Ther.*, 2001, **299**, 775–781.
125 H. Maeda, *Proc. Jpn. Acad. Ser. B: Phys. Biol. Sci.*, 2012, **88**, 53–71.
126 M. Gao, F. B. Yu, C. J. Lv, J. Choo and L. X. Chen, *Chem. Soc. Rev.*, 2017, **46**, 2237–2271.
127 K. D. Wegner and N. Hildebrandt, *Chem. Soc. Rev.*, 2015, **44**, 4792–4834.
128 J. Nicolas, S. Mura, D. Brambilla, N. Mackiewicz and P. Couvreur, *Chem. Soc. Rev.*, 2013, **42**, 1147–1235.
129 Y. Zhang, W. Xiu, Y. Sun, D. Zhu, Q. Zhang, L. Yuwen, L. Weng, Z. Teng and L. Wang, *Nanoscale*, 2017, **9**, 15835–15845.
130 B. L. Li, M. I. Setyawati, L. Y. Chen, J. P. Xie, K. Ariga, C. T. Lim, S. Garaj and D. T. Leong, *ACS Appl. Mater. Interfaces*, 2017, **9**, 15286–15296.